

Dilution impacts on smoke aging: Evidence in BBOP data

Anna L. Hodshire¹, Emily Ramnarine¹, Ali Akherati², Matthew L. Alvarado³, Delphine K. Farmer⁴, Shantanu H. Jathar², Sonia M. Kreidenweis¹, Chantelle R. Lonsdale³, Timothy B. Onasch⁵, Stephen R. Springston⁶, Jian Wang^{6,a}, Yang Wang^{7,b}, Lawrence I. Kleinman⁶, Arthur J. Sedlacek III⁶, Jeffrey R. Pierce¹

¹Department of Atmospheric Science, Colorado State University, Fort Collins, CO 80523, United States

²Department of Mechanical Engineering, Colorado State University, Fort Collins, CO 80523, United States

³Atmospheric and Environmental Research, Inc., Lexington, MA 02421, United States

⁴Department of Chemistry, Colorado State University, Fort Collins, CO 80523, United States

⁵Aerodyne Research Inc., Billerica, MA 01821, United States

⁶Environmental and Climate Sciences Department, Brookhaven National Laboratory, Upton, NY 11973, United States

⁷Center for Aerosol Science and Engineering, Washington University, St. Louis, MO 63130, United States

^aNow at Center for Aerosol Science and Engineering, Washington University, St. Louis, MO 63130, United States

^bNow at Department of Civil, Architectural and Environmental Engineering, Missouri University of Science and Technology, Rolla, Missouri 65409, United States

Correspondence to: Anna L. Hodshire (Anna.Hodshire@colostate.edu)

Abstract. Biomass burning emits vapors and aerosols into the atmosphere that can rapidly evolve as smoke plumes travel downwind and dilute, affecting climate- and health-relevant properties of the smoke. To date, theory has been unable to explain observed variability in smoke evolution. Here, we use observational data from the BBOP field campaign and show that initial smoke organic aerosol mass concentrations can help predict changes in smoke aerosol aging markers, number concentration, and number-mean diameter between 40-262 nm. Because initial field measurements of plumes are generally >10 minutes downwind, smaller plumes will have already undergone substantial dilution relative to larger plumes and have lower concentrations of smoke species at these observations closest to the fire. The extent to which dilution has occurred prior to the first observation is not a directly measurable quantity. Hence, initial observed plume concentrations can serve as a rough indicator of the extent of dilution prior to the first measurement, which impacts photochemistry, aerosol evaporation, and coagulation. Cores of plumes have higher concentrations than edges. By segregating the observed plumes into cores and edges, we find evidence that particle aging, evaporation, and coagulation occurred before the first measurement. We further find that on the plume edges, the organic aerosol is more oxygenated while a marker for primary biomass burning aerosol

40 emissions has decreased in relative abundance than in the plume cores. Finally, we attempt to decouple the roles of the
41 initial concentrations and time since emission by performing multivariate linear regression of various aerosol properties
42 (composition, size) on these two factors.

43 1 Introduction

44 Smoke from biomass burning is a major source of atmospheric primary aerosol and vapors (Akagi et al., 2011;
45 Gilman et al., 2015; Hatch et al., 2015, 2017; Jen et al., 2019; Koss et al., 2018; Reid et al., 2005; Yokelson et al., 2009),
46 influencing air quality, local radiation budgets, cloud properties, and climate (Carrico et al., 2008; O'Dell et al., 2019; Petters
47 et al., 2009; Ramnarine et al., 2019; Shrivastava et al., 2017), as well as the health of impacted communities (Ford et al.,
48 2018; Gan et al., 2017; Reid et al., 2016). Dilution of a smoke plume occurs as the plume ~~travels downwind, mixing~~ with
49 regional 'background' air, reducing the concentrations of the smoke aerosols and vapors and potentially driving changes in
50 the physical and chemical properties of the emissions (Adachi et al., 2019; Akagi et al., 2012; Bian et al., 2017; Cubison et
51 al., 2011; Hecobian et al., 2011; Hodshire et al., 2019a, 2019b; Jolleys et al., 2012, 2015; Konovalov et al., 2019; May et al.,
52 2015; Noyes et al., 2020; Sakamoto et al., 2015, Palm et al., 2020). Fires span an immense range in size, from small
53 agricultural burns, which may be only a few m² in total area and last a few hours, to massive wildfires, which may burn
54 10,000s of km² over the course of weeks (Andela et al., 2019). This range in size leads to variability in initial plume size and
55 extent of dilution by the time of the first measurement. Large, thick plumes dilute more slowly than small, thin plumes for
56 similar atmospheric conditions, as the cores of larger plumes are at a greater physical distance to the background air,
57 shielding them from dilution for longer (Akagi et al., 2012; Bian et al., 2017; Cubison et al., 2011; Hecobian et al., 2011;
58 Hodshire et al., 2019a, 2019b; Jolleys et al., 2012, 2015; Konovalov et al., 2019; May et al., 2015; Sakamoto et al., 2015,
59 Lee et al., 2020, Garofalo et al., 2019). Plumes can dilute unevenly, with edges of the plume mixing in with surrounding air
60 more rapidly than the core of the plume. Variability in dilution leads to variability in the evolution of smoke emissions as
61 instantaneous plume aerosol concentrations will control shortwave radiative fluxes (and thus photolysis rates and oxidant
62 concentrations), gas-particle partitioning, and particle coagulation rates (Akagi et al., 2012; Bian et al., 2017; Cubison et al.,
63 2011; Hecobian et al., 2011; Hodshire et al., 2019a, 2019b; Jolleys et al., 2012, 2015; Konovalov et al., 2019; May et al.,
64 2015; Sakamoto et al., 2015, Garofalo et al., 2019, Ramnarine et al., 2019; Sakamoto et al., 2016). Thus, capturing
65 variability in plume aerosol concentrations and dilution between fires and within fires can aid in understanding how species
66 change within the first few hours of emission for a range of plume sizes.

67 The evolution of total particulate matter (PM) or organic aerosol (OA) mass from smoke has been the focus of
68 many studies, as PM influences both human health and climate. Secondary organic aerosol (SOA) production occurs through
69 oxidation of gas-phase volatile organic compounds (VOCs) that can form lower-volatility products that partition to the
70 condensed phase (Jimenez et al., 2009; Kroll and Seinfeld, 2008). SOA formation may also arise from heterogeneous and
71 multi-phase reactions in both the organic and aqueous phases (Jimenez et al., 2009; Volkamer et al., 2009). In turn, oxidant

72 concentrations depend on shortwave fluxes (Tang et al., 1998; Tie, 2003; Yang et al., 2009) and the composition of the
73 plume (Yokelson et al. 2009; Akagi et al. 2012; Hobbs et al. 2003; Alvarado et al. 2015). Smoke particles contain
74 semivolatile organic compounds (SVOCs) (Eatough et al., 2003; May et al., 2013), which may evaporate off of particles as
75 the plume becomes more dilute (Huffman et al. 2009; May et al. 2013; Garofalo et al. 2019; Grieshop et al. 2009), leading to
76 losses in total aerosol mass. Field observations of smoke PM and OA mass normalized for dilution (e.g. through an inert
77 tracer such as CO) report that for near-field (<24 hours) physical aging, net PM or OA mass can increase (Cachier et al.,
78 1995; Formenti et al., 2003; Liu et al., 2016; Nance et al., 1993; Reid et al., 1998; Vakkari et al., 2014, 2018; Yokelson et al.,
79 2009), decrease (Akagi et al., 2012; Hobbs et al., 2003; Jolleys et al., 2012, 2015; May et al., 2015), or remain nearly
80 constant (Brito et al., 2014; Capes et al., 2008; Collier et al., 2016; Cubison et al., 2011; Forrister et al., 2015; Garofalo et al.,
81 2019; Hecobian et al., 2011; Liu et al., 2016; May et al., 2015; Morgan et al., 2019; Sakamoto et al., 2015; Sedlacek et al.,
82 2018; Zhou et al., 2017). It is theorized that both losses and gains in OA mass are likely happening concurrently in most
83 plumes through condensation and evaporation (May et al. 2015; Hodshire et al. 2019; Hodshire et al. 2019; Bian et al. 2017;
84 Palm et al. 2020), with the balance between the two determining whether net increases or decreases or no change in mass
85 occurs during near-field aging. However, there is currently no reliable predictor of how smoke aerosol mass (normalized for
86 dilution) may change for a given fire.

87 Evolution of total aerosol number, size, and composition is critical for improving quantitative understanding of how
88 biomass burn smoke plumes impact climate. These impacts include smoke aerosols' abilities to both act as cloud
89 condensation nuclei (CCN) and to scatter/absorb solar radiation, ~~each of which is determined by particle size and~~
90 ~~composition~~ (Albrecht, 1989; Petters and Kreidenweis, 2007; Seinfeld and Pandis, 2006; Twomey, 1974; Wang et al., 2008).
91 Particles can increase or decrease in size as well as undergo compositional changes through condensation or evaporation of
92 more volatile compounds. In contrast, coagulation always decreases total number concentrations and increases average
93 particle diameter. Plumes with higher aerosol number concentrations will undergo more coagulation than those with lower
94 concentrations (Sakamoto et al., 2016).

95 Being able to predict smoke aerosol mass, number, size, and composition accurately is an essential component in
96 constraining the influence of fires on climate, air quality, and health. Fires in the western United States region are predicted
97 to increase in size, intensity, and frequency (Dennison et al., 2014; Ford et al., 2018; Spracklen et al., 2009; Yue et al.,
98 2013). In response, several large field campaigns have taken place in the last 7 years examining wildfires in this region
99 (Kleinman et al., 2020; Garofalo et al. 2019; Palm et al., 2020). Here, we present smoke plume observations from the
00 Biomass Burning Observation Project (BBOP) campaign of aerosol properties from five research flights sampling wildfires
01 downwind in seven pseudo-Lagrangian sets of transects to investigate the evolution of OA mass and oxidation state, aerosol
02 number, and aerosol number mean diameter. A range of initial (at the time of the first plume pass in the aircraft) plume OA
03 mass concentrations were captured within these flights and fast (1 second) measurements of aerosols and key vapors were
04 taken. The time resolution of the data was great enough ~~that we have been able~~ to segregate each transect into edge, core, or
05 intermediate regions of the plume and examine aerosol properties within the context of both the location within the plume

06 (edge, core, or intermediate) and the initial OA mass loading of the ~~given location~~. The differences in aerosol loading serve
07 as a proxy for differences in initial fire and plume sizes, mass fluxes, and subsequent amount of dilution. The extent to which
08 dilution has occurred prior to the first observation is not a measurable quantity, and fire sizes and mass fluxes were not
09 estimated as a part of the BBOP campaign. We create mathematical fits for predicting OA oxidation markers and mean
10 particle diameter given initial plume OA mass concentration and physical age (time) of the smoke. These fits may be used to
11 evaluate other smoke datasets and assist in building parameterizations for regional and global climate models to better-
12 predict smoke aerosol climate and health impacts.

13 2 Methods

14 The BBOP field campaign occurred in 2013 and included a deployment of the United States Department of Energy
15 Gulfstream 1 (G-1) research aircraft in the Pacific Northwest region of the United States (Kleinman and Sedlacek, 2016;
16 Sedlacek et al., 2018) from June 15 to September 13. We analyze five cloud-free BBOP research flights that had seven total
17 sets of across-plume transects that followed the smoke plume downwind in a Lagrangian manner (see Figs. S1-S6 for
18 examples; Table S1) from approximately 15 minutes after emission to 2-4 hours downwind (Kleinman and Sedlacek, 2016).
19 The G-1 sampling setup is described in (Kleinman and Sedlacek, 2016; Sedlacek et al., 2018; Kleinman et al., 2020).

20 Number size distributions were obtained with a Fast-integrating Mobility Spectrometer (FIMS), providing particle
21 size distributions nominally from approximately 20-350 nm (Kulkarni and Wang, 2006; Olfert and Wang, 2009); data was
22 available between 20-262 nm for the flights used in this study. A Soot Photometer Aerosol Mass Spectrometer (SP-AMS)
23 provided organic and inorganic (sulfate, chlorine, nitrate, ammonium) aerosol mass concentration of PM1 (sub-micron
24 aerosol) (Canagaratna et al. 2007), select fractional components (the fraction of the AMS OA spectra at a given mass-to-
25 charge ratio) (Onasch et al., 2012), and elemental analysis (O/C and H/C) (Aiken et al., 2008; Canagaratna et al., 2015).
26 Extended details on the SP-AMS are provided in Text S1 in the supplementary information, and a brief overview is given
27 here. The SP-AMS had its highest sensitivity between 70-500 nm, dropping to 50% of peak sensitivity by 1000 nm (Liu et
28 al. 2007). It was characterized to have a collection efficiency of 0.5 when the instrument's laser was off and 0.76 when the
29 instrument's laser was on during the BBOP campaign, and these corrections have been applied to the data. There is evidence
30 from other studies that the CE of the tungsten vaporizer (laser off mode) (Lim et al., 2019) and the laser vaporizer (laser on
31 mode) (Willis et al., 2014) to change as a function of chemical composition, rBC coating thickness, size, and sphericity in
32 laboratory studies (Middlebrook et al., 2012; Willis et al., 2014; Corbin et al., 2015; Massoli et al., 2015; Collier et al., 2018)
33 and in aircraft observations (Kleinman et al. 2007). Results pertinent to changes in CE due to aging in smoke plumes are
34 scarce (see discussion in Kleinman et al., 2020). We assume these CEs for the laser on and off modes are constant in space
35 and time, which is a limitation of this study. We use the calculated f_{60} and f_{44} fractions (the mass concentrations of m/z 60
36 and 44 normalized by the total OA mass concentration) and O/C and H/C elemental ratios of OA as tracers of smoke and
37 oxidative aging. Elevated f_{60} values are indicative of "levoglucosan-like" species (levoglucosan and other molecules that

38 similarly fragment in the AMS) (Aiken et al., 2009; Cubison et al., 2011; Lee et al., 2010) and are known tracers of smoke
39 primary organic aerosol (POA) (Cubison et al., 2011). f_{44} , the OA fractional component observed by the SP-AMS as the ion
40 fragment CO₂⁺ as well as some acid groups, is a proxy for SOA arising from oxidative aging (Alfarra et al., 2004; Cappa
41 and Jimenez, 2010; Jimenez et al., 2009; Volkamer et al., 2006). Fractional components f_{60} and f_{44} have been shown to
42 decrease and increase with photochemical aging, respectively, likely due to both evaporation and/or oxidation of
43 semivolatile species that contribute to m/z 60 in the SP-AMS and addition of oxidized species that contribute to m/z 44 in
44 the SP-AMS (Alfarra et al., 2004; Huffman et al., 2009). O/C tends to increase with oxidative aging (Decarlo et al., 2008)
45 whereas H/C ranges from increasing to decreasing with oxidative aging, depending on the types of reactions occurring
46 (Heald et al., 2009). Changes in O/C and H/C (as well as changes in total OA mass, number, f_{44} , and f_{60}) are also
47 influenced by mixing of different air masses and co-oxidation of different VOC precursors (Chen et al. 2015). Tracking H/C
48 with aging may provide clues upon the types of reactions that may be occurring; however, variable oxidation timescales can
49 make inferences of this type difficult (Chen et al. 2015). A Single-Particle Soot Photometer (SP2; Droplet Measurement
50 Technologies) was used to measure refractory black carbon (BC) between 80-500 nm (Schwarz et al. 2010) through laser-
51 induced incandescence (Moteki and Kondo, 2010; Schwarz et al., 2006). An Off-Axis Integrated-Cavity Output
52 Spectroscopy instrument (Los Gatos, Model 907) measured CO concentrations. An SPN1 radiometer (Badosa et al., 2014;
53 Long et al., 2010) measured total shortwave irradiance. Kleinman et al. (2020) provides extensive details for the BBOP
54 instruments used in this work. The supporting information also includes more details on the instruments used.

55 To determine the contribution to the concentration of species X from smoke emissions (ΔX), the background
56 concentration of X is subtracted off of the measured in-plume species concentrations. To correct for dilution, we normalize
57 ΔX by background-corrected CO (ΔCO), which is inert on timescales of near-field aging (Yokelson et al., 2009). Increases
58 or decreases of $\Delta X/\Delta CO$ along the Lagrangian flight path indicate whether the total amount of X in the plume has increased
59 or decreased (implying production or removal) since time of emission. The background concentration of X is determined as
60 a regional average of the observed out-of-plume concentrations of X. To avoid using smoke-impacted measurements we
61 apply a threshold of only using measurements of X that occur in regions that correspond to the lowest 10% of CO data. We
62 determine the lowest 10% of CO concentrations from each flight during time periods with a similar altitude, latitude, and
63 longitude as the smoke plume. We perform sensitivity calculations on our assumptions of background regions and discuss
64 them in Section 3.

65 Mass concentrations of O, H, and C are calculated using the O/C and H/C and OA data from the SP-AMS
66 (assuming all of the OA mass is from O, C, and H), allowing us to calculate the background-corrected OA atomic ratios,
67 $\Delta O/\Delta C$, and $\Delta H/\Delta C$, following equation 1 (where X = O or H):

$$68 \frac{\Delta X}{\Delta C} = \frac{(X_{in\ plume} - X_{out\ of\ plume})}{(C_{in\ plume} - C_{out\ of\ plume})} \quad \text{Eq. 1}$$

69 We note that any non-linear changes in chemistry and composition between the plume and background will not perfectly
70 isolate the elemental factors in smoke. We also background-correct fractional f_{60} and f_{44} (using the mass concentrations of

71 m/z 60, m/z 44, and OA inside and outside of the plume), but we do not normalize by CO due to these values already being
72 normalized by OA, following equation 2 (where $f = f_{60}$ or f_{44}):

$$73 \Delta f = \frac{(f_{in} * OA_{in}) - (f_{out} * OA_{out})}{\Delta OA} \quad \text{Eq. 2}$$

74 We only consider data to be in-plume if the absolute CO ≥ 150 ppbv. This threshold appears to be capturing clear plume
75 features as seen in the number concentration while excluding background air (Figs. S7-S11). We note that we use different
76 definitions of in-plume and background (i.e. the lowest 10% of CO measurements) in order to provide a buffer between the
77 plume and background to ensure to the best of our abilities that we are capturing non-smoke impacted air for the background
78 and smoke-impacted air for in-plume cases. The regions of the lowest 10% of CO measurements always fall under 150 ppbv
79 (Figs. S7-S11). Similarly, we exclude the lowest 5% of CO data in the in-plume measurements in our analyses to provide a
80 further buffer between smoke-impacted and background air. We perform sensitivity analyses of our results to our
81 assumptions about background and in-plume values in Section 3. Figures S2-S6 indicate the locations of the lowest 10% of
82 CO for each flight.

83 From the FIMS, we examine the background-corrected, normalized number concentrations of particles with
84 mobility diameters between 40-262 nm, $\Delta N / \Delta CO$. This size range allows us to exclude potential influence of fresh
85 nucleation upon the total number concentrations. Occasionally, the background-corrected, normalized number concentration
86 in the FIMS size range between 20-40 nm increases by 1-2 orders of magnitude relative to typical plume conditions,
87 indicating possible nucleation events, primarily at the edges or in between smoke plumes (Figs. S7-S11). Smoke plumes
88 contain particles with diameters larger than 262 nm (Janhäll et al., 2009): thus, we cannot provide total number
89 concentrations, but we can infer how $\Delta N / \Delta CO$ within our observed size range evolves. We also obtain an estimate of how
90 the number mean diameter between 40-262 nm, \overline{D}_p , changes with aging through:

$$92 \overline{D}_p = \frac{\sum N_i * D_{p,i}}{\sum N_i} \quad \text{Eq. 3}$$

93
94 where N_i and $D_{p,i}$ are the number concentration and geometric mean diameter within each FIMS size bin, respectively.

95 All of the data are provided at 1 Hz and all but the SP-AMS fractional component data are available on the DOE
96 ARM web archive (<https://www.arm.gov/research/campaigns/aaf2013bbop>). As the plane traveled at approximately 100 m
97 s⁻¹ on average, data were collected every 100 m across the plume. The plumes spanned from approximately 5-50 km wide
98 (Figs. S2-6). The instruments used here had a variety of time lags (all <10 seconds) relative to a TSI 3563 nephelometer used
99 as reference. The FIMS also showed additional smearing in flushing smoky air with cleaner air when exiting the plume with
100 maximum observed flushing timescales around 30 seconds, but generally less (Fig. S12). To test if these lags impact our
101 results, we perform an additional analysis where we only consider the first half of each in-plume transect, when
102 concentrations are generally rising with time (Figure S12-S13), and our main conclusions are unaffected. We do not test the

03 impacts of other time lags and do not attempt to further correct the data for any time lags. Kleinman et al. (2020) provides
04 further information on instrument time delays during BBOP.

05 We use MODIS Terra and Aqua fire and thermal anomalies detection data to determine fire locations (Giglio et al.,
06 2006, 2008). We estimate the fire center to be the approximate center of all clustered MODIS detection points for a given
07 sampled fire (Figs. S1-S6). The true fire location at the time of sampling is likely different than the MODIS estimates,
08 depending on the speed of the fire front. To estimate the physical age of the plume, we use the estimated fire center as well
09 as the total FIMS number concentration to determine an approximate centerline of the plume as the smoke travels downwind
10 (an example is provided in Fig. S1). The centerline is subjectively chosen to approximately capture the **most-concentrated**
11 portion of each plume pass (as estimated using total aerosol number concentrations). We use the mean wind speed and this
12 estimated centerline to calculate an estimated physical age for each transect, and this physical age is assumed to be constant
13 across the transect, ~~as plume crossings took between 50-500 seconds; however,~~ transects that were not perfectly tangential to
14 the mean wind would have sampled different plume ages on the opposite sides of the plume. We did not propagate
15 uncertainty in fire location, wind speed, or centerline through to the physical age, which is a limitation of this study.

16 3 Results and discussion

17 As a case example, we examine the aging profiles of smoke from the Colockum fire during the first set of pseudo-
18 Lagrangian transects for flight 730b (Table S1). Figure 1 provides $\Delta\text{OA}/\Delta\text{CO}$, $\Delta\text{BC}/\Delta\text{CO}$, Δf_{60} , Δf_{44} , $\Delta\text{H}/\Delta\text{C}$, $\Delta\text{O}/\Delta\text{C}$,
19 $\Delta\text{N}/\Delta\text{CO}$, and $\overline{D_p}$ as a function of the estimated physical age; Figs. S14-S18 provides this information for the other pseudo-
20 Lagrangian transect flight sets studied. (Here, BC represents the refractory BC from the SP2; Sect. 2.) We have divided each
21 transect into four regions: between the 5-15 (edge), 15-50 (intermediate, outer), 50-90 (intermediate, inner), and 90-100
22 (core) percentile of ΔCO within each transect. (As discussed above, we exclude the lowest 5% in order to provide a buffer
23 between the plume edge and background air.) Note that in Figure 1 (and Figures S14-S18), the points represent the mean
24 values for each transect/percentile and do not include error bars for ~~uncertainty in the mean~~ or measurement uncertainty as
25 **characterization of systematic variance (within plume percentiles) with age is beyond the scope of this study**. Figures S2-S6
26 show the locations of these CO percentile bins for each transect of individual flights. Figure 1 shows the edge and core data,
27 both averaged per transect, and Figs. S14-18 provides all four percentile bins for each flight. These percentile bins correspond
28 with the thinnest (lowest CO mixing ratio) to thickest (highest CO mixing ratio) portions of the plume, respectively. **If a fire**
29 **has uniform emissions ratios across all regions and dilutes evenly downwind, these percentile bins would correspond to the**
30 **edges, intermediate regions, and the core of the diluting plume.** We use this terminology in this study but note that uneven
31 emissions, mixing, and/or dilution lead to the percentile bins not physically corresponding to our defined regions in some
32 cases. We note that some plumes show more than one maxima in CO concentrations within a given plume crossing, which
33 implies that there may be more than one fire or fire front, and that these plumes from separate fires or fronts are not mixing
34 perfectly. Multiple maxima could also imply vertical variations in the location of the core of the plumes that the flights did

35 not capture. As well, in at least one of the fires (in flights ‘730a’ and ‘730b’), the fuels vary between different sides of the
36 fire, as discussed in Kleinman et al., (2020). However, the lowest two ΔCO bins tend ~~more~~ towards the physical edges of the
37 plume, and the highest two tend more towards the physical center of the plume (Figs. S2-S6). We do not know where the
38 plane is vertically in the plume, which is a limitation as vertical location will also impact the amount of solar flux able to
39 penetrate through the plume.

40 Figure 1 shows that for this specific plume, $\Delta\text{OA}/\Delta\text{CO}$ and $\Delta\text{BC}/\Delta\text{CO}$ systematically vary little with age for both
41 the 5-15 and 90-100 percentile of ΔCO (p-values>0.5), yet both show non-systematic variability between transects. A true
42 Lagrangian flight with the aircraft sampling the same portion of the plume and no measurement artifacts (e.g. coincidence
43 errors at high concentrations) would have a constant $\Delta\text{BC}/\Delta\text{CO}$ for each transect set. This flight and other flights studied
44 here have variations in $\Delta\text{BC}/\Delta\text{CO}$ (Fig. 1; Figs. S14-S18), which may be indicative of deviations from a Lagrangian flight
45 path with temporal variations in emission and/or measurement uncertainties. The remaining variables plotted also show some
46 noise and few clear trends, but it is apparent that the transect-mean values 5-15 and 90-100 percentiles do show a separation
47 for some of the individual metrics, in particular Δf_{44} and $\Delta\text{O}/\Delta\text{C}$. In order to determine the existence or lack of trends for
48 these metrics, we spend the remainder of this study examining each metric from all of the pseudo-Lagrangian flights
49 together.

50

51 3.1 Organic aerosol aging: $\Delta\text{OA}/\Delta\text{CO}$, Δf_{60} , Δf_{44} , $\Delta\text{H}/\Delta\text{C}$, and $\Delta\text{O}/\Delta\text{C}$

52 Figure 2a-e shows available $\Delta\text{OA}/\Delta\text{CO}$, Δf_{60} , Δf_{44} , $\Delta\text{H}/\Delta\text{C}$, and $\Delta\text{O}/\Delta\text{C}$ edge and core data versus physical age for
53 each transect for each flight of this study. We color each line by the mean ΔOA within a ΔCO percentile bin from the
54 transect closest to the fire, $\Delta\text{OA}_{\text{initial}}$, in order to examine whether each variable ($\Delta\text{OA}/\Delta\text{CO}$, Δf_{60} , Δf_{44} , $\Delta\text{H}/\Delta\text{C}$, and
55 $\Delta\text{O}/\Delta\text{C}$) vary with $\Delta\text{OA}_{\text{initial}}$. (Some transects do not have data available for specific instruments.) As with Fig. 1, the
56 points in Fig. 2 represent the mean values for each transect and percentile, and we do not include error bars as we do not
57 attempt to characterize systematic variance (within plume percentiles) with age in this study. We note that $\Delta\text{OA}_{\text{initial}}$ does not
58 actually represent the true initial emitted OA from each fire, but instead serves as a proxy for the general fire size, intensity,
59 and emission rate (as larger fires and fires with faster rates of fuel consumption per area will have larger mass fluxes than
60 smaller fires or fires with less fuel consumption per area, all else equal). Thus, $\Delta\text{OA}_{\text{initial}}$ and other “initial” metrics referred
61 to in this study are not to be taken as emission values and direct comparison to studies with direct emissions values is not
62 appropriate, as dilution and chemistry may occur before the initial flight transect, which we discuss further below. We show
63 the 5-15 (edge) and 90-100 (core) ΔCO percentile bins in Fig. 2; Fig. S19 shows the same information for all four ΔCO
64 percentiles. We use the simple ‘edge’ and ‘core’ terminology throughout the following discussion but note that the 5-15 and
65 90-100 ΔCO percentile bins do not necessarily correspond to the physical (spatial) edges and cores of each plume. They
66 instead correspond to the most CO-dense and least CO-dense portions of the plume. We also note that although some of the
67 physical ages appear to start at approximately 0 hours (e.g. over the fire), this is from a limitation of our physical age

68 estimation method (Sect. 2), as no flights captured data before approximately 15 minutes after emission (Kleinman et al.,
69 2016). Flights with two sets of pseudo-Lagrangian transects ('726a' and '730b') have two separate lines in Fig. 2, one for
70 each set. As well, two transects for flight '809a' nearly overlap (Fig. S5), with the transect that is further from the fire
71 occurring first in the flight path, leading to an apparent slight decrease in physical age for the sequential transect (see, e.g.,
72 the white dashed line in Fig. 2a).

73 Also included in Fig. 2 are the Spearman rank-order correlation tests (hereafter Spearman tests), which are tests for
74 monotonicity. The Spearman tests show correlation coefficients for each flight set (Table S1) with the initial ΔOA of a flight
75 set ($\Delta\text{OA}_{\text{initial}}$) against $\Delta\text{OA}/\Delta\text{CO}$, Δf_{60} , Δf_{44} , $\Delta\text{H}/\Delta\text{C}$, and $\Delta\text{O}/\Delta\text{C}$ as the smoke aerosol ages downwind. We also include
76 Spearman tests for the calculated physical age of the smoke for each flight set against these same variables. The R values are
77 labeled $R_{\Delta\text{OA},\text{initial}}$ and R_{age} , respectively, in Fig. 2. We calculate these correlation coefficients separately for Figure 2 to
78 determine how well variability for each variable can be predicted from the $\Delta\text{OA}_{\text{initial}}$ or age alone (and whether the data are
79 correlated vs. anticorrelated with these predictors). To complement these independent correlation coefficients, we also
80 perform multivariate linear regressions (Eqns. 4 and 5 and Figure 3, discussed later) to explicitly decouple the influence of
81 the two predictors. For the correlations with $\Delta\text{OA}_{\text{initial}}$, all transects in a given pseudo-Lagrangian set of transects have the
82 same $\Delta\text{OA}_{\text{initial}}$ value; for flights with two pseudo-Lagrangian sets of transects, each set has its own $\Delta\text{OA}_{\text{initial}}$ value.
83 Correlating to $\Delta\text{OA}_{\text{initial}}$ provides an estimate of how the plume aerosol concentrations at the time of the initial transect
84 impact plume aging (aging both before and after this initial transect). We define the following categories of correlation for
85 the absolute value of R: 0.0-0.19 is 'very weak', 0.2-0.39 is 'weak', 0.4-0.59 is 'moderate', 0.6-0.79 is 'strong', and 0.8-1.0
86 is 'very strong' (Evans 1996).

87 As individual flights show scatter in the metrics of Fig. 2 (Figs. 1, Figs. S14-S18), we also include $R_{\Delta\text{OA},\text{initial}}$ and
88 R_{age} for each metric of Fig. 2 sequentially removing one flight from the statistical analysis. These results are summarized in
89 Table S2. In general, removing single flights does not change our conclusions, particularly when correlations are moderate or
90 stronger. Scatter in $\Delta\text{OA}_{\text{initial}}$ leads to weaker R_{age} values than would be obtained if we normalized changes with aging to the
91 first (normalized) value. However, as plume-density-dependent aging prior to the first transect is one of the potentially
92 interesting findings of this study, we feel that it is important to not normalize our changes further. Figs. S13, S19-S22 show
93 the same details as Fig. 2 but provide sensitivity tests to our methodology. Figure S13 examines potential FIMS
94 measurement artifacts by only using data from the first 50% of each flight leg when particle concentrations are increasing,
95 which lessons response-time-artifacts of the FIMS during transitions from high to low concentration regions. Figure S20
96 tests our assumed in-plume CO threshold value by increasing it from 150 ppbv to 200 ppbv (Fig. S19). Figure S21 tests
97 ΔCO percentile spacing by changing the bins from 5-15%, 15-50%, 50-90%, and 90-100% to 5-25%, 25-75%, and 75-100%.
98 Figure S22 tests assumed background region by increasing data used from the lowest 10% to the lowest 25% of CO
99 measurements. Although these figures show slight variability, the findings discussed below remain robust, and we constrain
00 the rest of our discussion to the original assumptions made for the FIMS measurements, in-plume CO threshold value, and
01 ΔCO percentiles used in Fig. 2.

02 In general, both the cores and edges do not show any positive or negative trend in $\Delta\text{OA}/\Delta\text{CO}$ with respect to
03 physical aging. The correlation coefficients, $R_{\Delta\text{OA},\text{initial}}$ and R_{age} , show very weak correlations of 0.02 and +0.03 (with
04 $R_{\Delta\text{OA},\text{initial}}$ and R_{age} ranging between -0.25 to +0.17 and 0 to 0.07, respectively, when individual flights are left out
05 sequentially; Table S2). The absolute variability in $\Delta\text{OA}/\Delta\text{CO}$ is dominated by differences between plumes. Many previous
06 field campaigns similarly show little change in $\Delta\text{OA}/\Delta\text{CO}$ with aging (Hodshire et al., 2019a and references therein; Palm et
07 al., 2020). This may be due to a balance between evaporation and condensation over the period of time that the plume is
08 observed (Hodshire et al., 2019a). This hypothesis is supported by the observed Δf_{60} and Δf_{44} . The fractional components
09 Δf_{60} and Δf_{44} show clear signs of changes with aging, consistent with previous studies (Cubison et al. 2011; May et al. 2015;
10 Garofalo et al. 2019; Forrister et al. 2015; Lee et al. 2020). Δf_{60} generally decreases with plume age ($R_{\text{age}} = -0.26$; a weak
11 correlation), consistent with the hypotheses that compounds containing species that can fragment to m/z 60 in the SP-AMS
12 may be evaporating because of dilution, undergoing heterogeneous oxidation to new forms that do not appear at m/z 60,
13 and/or having a decreasing fractional contribution due to condensation of other compounds. In contrast, Δf_{44} generally
14 increases with age ($R_{\text{age}} = +0.5$; a moderate correlation) for all plumes with available data. It appears for the plumes in this
15 study that although there is little change in $\Delta\text{OA}/\Delta\text{CO}$, loss of compounds such as those that contribute to f_{60} fragments (as
16 captured by the SP-AMS) is roughly balanced by condensation of more-oxidized compounds, including those that contain
17 compounds with f_{44} fragments, such as carboxylic acids. This observation also suggests the possibility of heterogeneous or
18 particle-phase oxidation that would alter the balance of Δf_{60} and Δf_{44} . However, estimates of heterogeneous mass losses
19 indicate that after three hours of aging (the range of time the BBOP measurements were taken in) for a range of OH
20 concentrations and reactive uptake coefficients, less than 10% of aerosol mass is lost to heterogeneous reactions (Fig. S23;
21 see SI text S2 for more details on the calculation). These calculations indicate that heterogeneous loss has limited effect on
22 aerosol composition or mass. Hence, the evaporation of compounds that contribute to m/z 60 in the SP-AMS being balanced
23 by gas-phase production of compounds that contribute to m/z 44 in the SP-AMS may be the more likely pathway. When
24 individual flights are left out sequentially, R_{age} ranges from -0.21 to -0.38 and +0.4 to +0.57 for Δf_{60} and Δf_{44} , respectively
25 (Table S2).

26 Two more important features of Δf_{60} and Δf_{44} can be seen within Fig. 2: (1) Δf_{60} and Δf_{44} depend on $\Delta\text{OA}_{\text{initial}}$
27 (moderate correlations of $R_{\Delta\text{OA},\text{initial}} = +0.43$ and -0.55, respectively), with plumes with higher $\Delta\text{OA}_{\text{initial}}$ having
28 consistently higher Δf_{60} and lower Δf_{44} . (2) The differences in Δf_{60} and Δf_{44} are apparent even for the nearest-to-source
29 measurements that are ~15 minutes after the time of emission. Prior studies have shown that f_{60} and f_{44} at the time of
30 emissions correlate with OA emissions factors through variability in burn conditions (Hennigan et al. 2011; Cubison et al.
31 2011; McClure et al. 2020), and this relationship might also contribute to our observed correlation between Δf_{60} and Δf_{44}
32 with $\Delta\text{OA}_{\text{initial}}$. For this emissions relationship to be an important factor, the variability in the OA emission factor needs to
33 be a significant contributor to the variability in $\Delta\text{OA}_{\text{initial}}$. If the relative variability in the OA emission factor is much
34 smaller than the relative variability in $\Delta\text{OA}_{\text{initial}}$, other factors contributing to variability in $\Delta\text{OA}_{\text{initial}}$ will negate an
35 emissions-based covariance between $\Delta\text{OA}_{\text{initial}}$ with Δf_{60} and Δf_{44} . While our observed $\Delta\text{OA}_{\text{initial}}$ in Figure 2 spans

36 nearly a factor of 100, Andreae (2019) shows that the OA emission factors have a -1σ to $+1\sigma$ range of around a factor 3.
37 Hence, variability in fuel consumption rates and dilution prior to the first transect likely dominate the variability in
38 $\Delta\text{OA}_{\text{initial}}$, and the relationships of Δf_{60} and Δf_{44} with $\Delta\text{OA}_{\text{initial}}$ are unlikely to be influenced much by variability in burn
39 conditions. We conclude that evaporation and/or chemistry prior to the first measurement appears to drive the initial
40 relationship between Δf_{60} and Δf_{44} with $\Delta\text{OA}_{\text{initial}}$, consistent with (1) the theoretical work of Hodshire et al. (2019a), (2)
41 an analysis of what chemistry would be missed in laboratory experiments if the initial 10-60 minutes of chemistry was not
42 considered, following field experiments (Hodshire et al., 2019b), and (3) recent field analysis indicating that up to one-third
43 of primary OA from biomass burning evaporates and subsequently reacts to form biomass burning SOA (Palm et al. 2020).
44 We include in the supporting information scatter plots of each parameter of Fig. 1 as a function of $\Delta\text{OA}_{\text{initial}}$ (Fig. S24), and
45 observe no trends other than the cores of the plumes generally having a higher $\Delta\text{OA}_{\text{initial}}$ than the edges of the plumes, as
46 expected. The amount of evaporation and/or chemistry appear to depend on $\Delta\text{OA}_{\text{initial}}$, with higher rates of evaporation and
47 chemistry occurring for lower values of $\Delta\text{OA}_{\text{initial}}$. This result is consistent with the hypothesis that aircraft observations are
48 missing evaporation and chemistry prior to the first aircraft observation (Hodshire et al., 2019b). The differences in $\Delta\text{OA}_{\text{initial}}$
49 between plumes may be due to different emissions fluxes (e.g., due to different fuels or combustion phases) or plume widths,
50 where larger/thicker plumes dilute more slowly than smaller/thinner plumes. These larger plumes have been predicted to
51 have less evaporation and may undergo relatively less photooxidation (Bian et al., 2017; Hodshire et al., 2019a, 2019b).
52 When individual flights are left out sequentially, $R_{\Delta\text{OA},\text{initial}}$ ranges from +0.3 to +0.58 and -0.42 to -0.63 for Δf_{60} and Δf_{44} ,
53 respectively (Table S2).

54 Garofalo et al. (2019) segregated smoke data from the WE-CAN field campaign by distance from the center of a
55 given plume and showed that the edges of one of the fires studied have less fractional f_{60} and more fractional f_{44} (not
56 background-corrected) than the core of the plume. Lee et al. (2020) saw similar patterns in a southwestern United States
57 wildfire. Similarly, we find that the 730b flight shows a very similar pattern in f_{60} and f_{44} (Figs. S25-S26) to that shown in
58 Fig. 6 of Garofalo et al. (2019). The 821b and 809a flights also hint at elevated f_{44} and decreased f_{60} at the edges but the
59 remaining plumes do not show a clear trend from the physical edges to cores in f_{60} and f_{44} . This could be as CO
60 concentrations (and thus presumably other species) do not evenly increase from the edge to the core for many of the plume
61 transects studied (Figs. S2-S6). To more clearly see this, Fig. S27 provides the same style of figure as Figs. S26-S27 for in-
62 plume CO concentrations. Generally CO peaks around the centerline and is highest in the most fresh transect, but shows
63 variability across transects. We do not have UV measurements that allow us to calculate photolysis rates but the in-plume
64 SPN1 shortwave measurements in the visible show a dimming in the fresh cores that has a similar pattern to f_{44} and the
65 inverse of f_{60} (Fig. S28; the rapid oscillations in this figure could be indicative of sporadic cloud cover above the plumes).
66 Lee et al. (2020) similarly saw indications of enhanced photochemical bleaching at the edges of a southwestern United States
67 wildfire when examining aerosol optical properties.

68 We also plot core and edge $\Delta\text{H}/\Delta\text{C}$ and $\Delta\text{O}/\Delta\text{C}$ as a function of physical age (Fig. 2d-e). Similar to Δf_{44} , $\Delta\text{O}/\Delta\text{C}$
69 increases with physical age and is well correlated to both physical age and $\Delta\text{OA}_{\text{initial}}$ (moderate correlations of $R_{\text{age}} = +0.561$

70 and $R_{\Delta OA, initial} = -0.45$). When individual flights are left out sequentially, R_{age} for $\Delta O/\Delta C$ ranges between +0.46 and +0.63
71 and $R_{\Delta OA, initial}$ ranges between -0.21 and -0.54 (Table S2). Given that Δf_{44} and $\Delta O/\Delta C$ are both metrics for OA aging (Sect.
72 2), it is unsurprising that we see similar trends between them. Conversely, $\Delta H/\Delta C$ is poorly correlated to physical age and
73 $\Delta OA_{initial}$.

74 Both physical age and $\Delta OA_{initial}$ appear to influence Δf_{60} , Δf_{44} , and $\Delta O/\Delta C$: oxidation reactions and evaporation
75 promoted by dilution occur with aging, and the extent of photochemistry and dilution should depend on plume thickness.
76 Being able to predict biomass burning aerosol aging parameters can provide a framework for interstudy-comparisons and can
77 aid in modeling efforts. We construct mathematical fits for predicting Δf_{60} , Δf_{44} , and $\Delta O/\Delta C$:

$$78 \quad X = a \log_{10}(\Delta OA_{initial}) + b (Physical\ age) + c \quad \text{Eq. 4}$$

80 where X is Δf_{60} , Δf_{44} , or $\Delta O/\Delta C$, physical age is in hours, and a , b , and c are fit coefficients. The measured versus fit data are
81 shown in Fig. 3a-c. The values of a , b , and c are provided in Table S3. The Pearson and Spearman coefficients of
82 determination (R_p^2 and R_s^2 , respectively) are also summarized in Fig. 3 and indicate weak-moderate goodness of fits (R_p^2 and
83 R_s^2 of 0.28 and 0.25 for Δf_{60} , R_p^2 and R_s^2 of 0.58 and 0.6 for Δf_{44} , and R_p^2 and R_s^2 of 0.45 and 0.55 for $\Delta O/\Delta C$). We show R^2
84 here to indicate the fraction of variability captured by these fits, whereas calculating R for the trends in Fig. 2 indicate the
85 direction of the correlation. We do not constrain our fits to go through the origin. To provide further metrics of goodness-of-
86 fit, we also include the normalized mean bias (NMB) and normalized mean error (NME) in percent for each metric of Fig. 3.
87 The NMB values are very close to zero (which is anticipated as linear fits seek to minimize the sum of squared residuals).
88 The NME is larger, at 19.8% for Δf_{60} , 14.9% for Δf_{44} , and 10.2% for $\Delta O/\Delta C$. The p-values for each fit are less than 0.01.
89 Although no models that we are aware of currently predict aerosol fractional components (e.g. f_{60} or f_{44}), O/H and H/C are
90 predicted by some models (e.g., Cappa and Wilson (2012)) and these fit parameters may assist in modeling of aging biomass
91 burning aerosol. Other functional forms for fits were explored, with the following form showing similar results as Eq. 4:
92

$$93 \quad \ln(\Delta X) = a \ln(\Delta OA_{initial}) + b \ln(Physical\ age) + c \quad \text{Eq. 5}$$

94 (Fig. S29 and Table S4 for the fit coefficients) and $\Delta N_{initial}$ in the place of $\Delta OA_{initial}$ in Eq. 4 (Fig. S30 and Table S5 for the fit
95 coefficients) providing similar correlation values and NMB and NME values for Δf_{60} , Δf_{44} , and $\Delta O/\Delta C$.

96 **The aging values of Δf_{60} , Δf_{44} , and $\Delta O/\Delta C$ show scatter** (Figs. S14-18), which likely contributes to the limited
97 predictive power of our mathematical fits. The scatter is likely due to variability in emissions due to source fuel or
98 combustion conditions, instrument noise and responses under the large concentration ranges encountered in these smoke
99 plumes, inhomogeneous mixing within the plume, variability in background concentrations not captured by our background
00 correction method, inaccurate characterizations of physical age due to variable wind speed, and/or deviations from a true
01 Lagrangian flight path. Eqs. 4-5 performed the best out of the mathematical fits that we tested. **These equations do not have a**
02
03

04 direct physical interpretation but may be used as a starting point for modeling studies as well as for constructing a more
05 physically based fit. There may be another variable not available to us in the BBOP measurements that can improve these
06 mathematical fits, such as photolysis rates. We do not know whether these fits may well-represent fires in other regions
07 around the world, given variability in fuels and burn conditions. We also do not know how these fits will perform under
08 nighttime conditions, as our fits were made for daytime conditions with different chemistry than would happen at night. We
09 encourage these fits to be tested with further data sets and modeling. These equations are a first step towards
10 parameterizations appropriate for regional and global modeling and need extensive testing to separate influences of oxidation
11 versus dilution-driven evaporation.

12 3.2 Aerosol size distribution properties: $\Delta N/\Delta CO$ and \overline{D}_p

13 The observations of the normalized number concentration between 40-262 nm, $\Delta N/\Delta CO$ (Fig. 2f), show that plume
14 edges and cores generally show decreases in $\Delta N/\Delta CO$ with physical age, with a weak correlation of $R_{\text{age}} = -0.27$ (-0.13 to -
15 0.43 when individual flights are left out, sequentially; Table S2). Although we would anticipate that plume regions with
16 higher initial ΔOA would have lower normalized number concentrations due to coagulation (Sakamoto et al. 2016), a few
17 dense cores have normalized number concentrations comparable or higher than the thinner edges, leading to no correlation
18 with $\Delta OA_{\text{initial}}$. We note that variability in number emissions (e.g., due to burn conditions) adds unexplained variability not
19 captured by the R values.

20 The mean particle size between 40-262 nm, \overline{D}_p (Eq. 3), is shown to statistically increase with aging when
21 considered across the BBOP dataset (Fig. 2g) (a moderate correlation of $R_{\text{age}} = +0.53$, with R_{age} ranging between +0.43 to
22 +0.63 when individual flights are left out sequentially; Table S2). Coagulation and SOA condensation will increase \overline{D}_p . OA
23 evaporation will decrease \overline{D}_p if the particles are in quasi-equilibrium (where evaporation is independent of surface area)
24 (Hodshire et al. 2019b). However, if evaporation is kinetically limited, smaller particles will preferentially evaporate more
25 rapidly than larger particles, which may lead to an increase in \overline{D}_p if the smallest particles evaporate below 40 nm (Hodshire
26 et al. 2019b). The plumes do not show significant changes in $\Delta OA/\Delta CO$ (Fig. 2a), indicating that coagulation is likely
27 responsible for the majority of increases in \overline{D}_p . (We acknowledge that $\Delta OA/\Delta CO$ may be impacted by measurement artifacts
28 as discussed in Sect. 2. For instance, if the collection efficiency of the AMS is actually decreasing with age, then $\Delta OA/\Delta CO$
29 would be increasing and the increases in number mean diameter will be due to SOA condensation as well as coagulation.)
30 We do not have measurements for the volatility of the smoke aerosol, and so cannot refine these conclusions further. We also
31 perform the functional fit analysis following Sect. 3.1 (Eq. 4; where X is \overline{D}_p in this case). The fit can also predict greater than
32 30 percent of the variance in \overline{D}_p (R_p^2 and R_s^2 of 0.37 and 0.33, NME of 5.5%, and p-value less than 0.01; Fig. 3d) but does
33 not predict $\Delta N/\Delta CO$ well (not shown). We show the functional fit for \overline{D}_p for the alternative fit equation (Eq. 5) in Fig. S29
34 and Table S4. We also show the functional fit for \overline{D}_p for Eq. 4 with $\Delta N_{\text{initial}}$ in place of $\Delta OA_{\text{initial}}$ in Fig. 30 and Table S5.
35 Sakamoto et al. (2016) provide fit equations for modeled \overline{D}_p as a function of age, but they include a known initial \overline{D}_p at the

36 time of emission in their parameterization (rather than 15 minutes or greater, as available to us in this study), which is not
37 available here. $\Delta N_{\text{initial}}$ in the place of $\Delta \text{OA}_{\text{initial}}$ in Eq. 4 predicts $\overline{D_p}$ similarly (Fig. S30). As discussed in Section 3.1, scatter
38 in number concentrations limits our prediction skill.

39 Particles appear in the 20-40 nm size range in the FIMS measurements independently of plume OA concentrations
40 (Figs S7-S11), implying that nucleation events may be occurring for some of the transects. Some pseudo-Lagrangian sets of
41 transects also show nucleation-mode particles downwind of fires in between transects (Figs. S7, S8, S9, and S11).
42 Nucleation-mode particles appear to be approximately one order of magnitude less concentrated than the larger particles, and
43 primarily occur in the outer portion of plumes, although one set of transects did show nucleation-mode particles within the
44 core of the plume (Fig. S11). Nucleation at edges could be due to increased photooxidation from higher total irradiance
45 relative to the core (Fig. S26). As well, nucleation is more favorable when the total condensation sink is lower (e.g. reduced
46 particle surface area; Dal Maso et al., 2002), which may occur for outer portions of plumes with little aerosol loading.
47 However, given the relatively small number of data points showing nucleation mode particles and limited photooxidation
48 and gas-phase information, we do not have confidence in the underlying source of the nucleation-mode particles.

49 4 Summary and outlook

50 The BBOP field campaign provided high time resolution (1 s) measurements of gas- and particle-phase smoke
51 measurements downwind of western U.S. wildfires along pseudo-Lagrangian transects. These flights have allowed us to
52 examine near-field (<4 hours) aging of smoke particles to provide analyses on how select species vary across a range of initial
53 organic aerosol mass loadings ($\Delta \text{OA}_{\text{initial}}$; a proxy for the relative rates at which the plume is anticipated to dilute as dilution
54 before the first observation is not a measurable quantity) as well as how the species studied vary between the edges and cores
55 of each plume. We find that although $\Delta \text{OA}/\Delta \text{CO}$ does not correlate with $\Delta \text{OA}_{\text{initial}}$ or physical age, Δf_{60} (a marker for
56 evaporation) is moderately correlated with $\Delta \text{OA}_{\text{initial}}$ (Spearman rank-order correlation tests correlation coefficient, $R_{\Delta \text{OA}, \text{initial}}$,
57 of +0.43) and weakly correlated with physical age (Spearman rank-order correlation tests correlation coefficient, R_{age} , of -
58 0.26). Δf_{44} and $\Delta \text{O}/\Delta \text{C}$ (markers for photochemical aging) increases with physical aging (moderate correlations of R_{age} of +0.5
59 and +0.56, respectively) and are inversely related to $\Delta \text{OA}_{\text{initial}}$ (moderate correlations of $R_{\Delta \text{OA}, \text{initial}}$ of -0.55 and -0.45,
60 respectively). $\Delta \text{N}/\Delta \text{CO}$ decreases with physical aging, likely through coagulation. Mean aerosol diameter increases with age
61 primarily due to coagulation, as organic aerosol mass does not change significantly, and is moderately correlated with physical
62 age ($R_{\text{age}} = +0.53$). Nucleation is observed within a few of the fires and appears to occur primarily on the edges of the plumes.
63 Differences in initial values of Δf_{60} , Δf_{44} , and $\Delta \text{O}/\Delta \text{C}$ are evidence that evaporation and/or chemistry has occurred before the
64 time of initial measurement and that plumes or plume regions with lower initial aerosol loading can undergo these changes
65 more rapidly than thicker plumes. We have developed fit equations that can weakly to moderately predict Δf_{60} , Δf_{44} , $\Delta \text{O}/\Delta \text{C}$,
66 and mean aerosol diameter given a known initial (at the time of first measurement) total organic aerosol mass loading and
67 physical age. We were unable to quantify the impact on potential inter-fire variability in the emission values of the metrics

68 studied here (such as variable emissions of species that can contribute to m/z 60 and m/z 44). We anticipate that being able
69 to capture this additional source of variability may lead to stronger fits and correlation. We encourage future studies to attempt
70 to quantify these chemical and physical changes before the initial measurement using combinations of modeling and laboratory
71 measurements, where sampling is possible at the initial stages of the fire and smoke. We also suggest further refinement of our
72 fit equations, as additional variables (such as photolysis rates) and better quantification of inter-fire variability (such as variable
73 emission rates) are anticipated to improve these fits. We finally urge future near-field (<24 hours) analyses of recent and future
74 biomass burning field campaigns to include differences in initial plume mass concentrations and location within the plume as
75 considerations for understanding chemical and physical processes in plumes.

76 **Acknowledgements**

77 We would like to thank Lauren Garofalo, Emily Fischer, Jakob Lindaas, and Ilana Pollack for useful conversations. We
78 thank Charles Long for use of irradiation data. This work is supported by the U.S. NOAA, an Office of Science, Office of
79 Atmospheric Chemistry, Carbon Cycle, and Climate Program, under the cooperative agreement awards NA17OAR4310001
80 and NA17OAR4310003; the U.S. NSF Atmospheric Chemistry program, under Grants AGS-1559607 and AGS-1950327;
81 and the US Department of Energy's (DOE) Atmospheric System Research, an Office of Science, Office of Biological and
82 Environmental Research program, under grant DE-SC0019000. Work conducted by LIK, AJS, JW was performed under
83 sponsorship of the U.S. DOE Office of Biological & Environmental Sciences (OBER) Atmospheric System Research
84 Program (ASR) under contracts DE-SC0012704 (BNL; LIK, AJS) and DE-SC0020259 (JW). Researchers recognize the
85 DOE Atmospheric Radiation Measurement (ARM) Climate Research program and facility for both the support to carry out
86 the BBOP campaign and for use of the G-1 research aircraft. TBO acknowledges support from the DOE ARM program
87 during BBOP and the DOE ASR program for BBOP analysis (contract DE-SC0014287). DKF acknowledges funding from
88 NOAA Climate Program Office's Atmospheric Chemistry, Carbon Cycle, and Climate program (Grant NA17OAR4310010).
89 We thank the anonymous reviewers for their constructive feedback.

90

93 **References**

- 94 Adachi, K., Sedlacek, A. J., Kleinman, L., Springston, S. R., Wang, J. and Chand, D.: Spherical tarball particles form
95 through rapid chemical and physical changes of organic matter in biomass-burning smoke, *Proceedings of the*
96 *National Academy of Sciences*, 1–6, 2019.
- 97 Aiken, A. C., Decarlo, P. F., Kroll, J. H., Worsnop, D. R., Huffman, J. A., Docherty, K. S., Ulbrich, I. M., Mohr, C.,
98 Kimmel, J. R., Sueper, D., Sun, Y., Zhang, Q., Trimborn, A., Northway, M., Ziemann, P. J., Canagaratna, M. R.,
99 Onasch, T. B., Alfarra, M. R., Prevot, A. S. H., Dommen, J., Duplissy, J., Metzger, A., Baltensperger, U. and
00 Jimenez, J. L.: O/C and OM/OC ratios of primary, secondary, and ambient organic aerosols with high-resolution
01 time-of-flight aerosol mass spectrometry, *Environmental Science and Technology*, 42(12), 4478–4485, 2008.
- 02 Aiken, A. C., Salcedo, D., Cubison, M. J., Huffman, J. A., DeCarlo, P. F., Ulbrich, I. M., Docherty, K. S., Sueper, D.,
03 Kimmel, J. R., Worsnop, D. R. and Others: Mexico City aerosol analysis during MILAGRO using high resolution
04 aerosol mass spectrometry at the urban supersite (T0)--Part 1: Fine particle composition and organic source
05 apportionment, *Atmos. Chem. Phys.*, 9(17), 6633–6653, 2009.
- 06 Akagi, S. K., Yokelson, R. J., Wiedinmyer, C., Alvarado, M. J., Reid, J. S., Karl, T., Crounse, J. D. and Wennberg, P. O.:
07 Emission factors for open and domestic biomass burning for use in atmospheric models, *Atmos. Chem. Phys.*,
08 11(9), 4039–4072, 2011.
- 09 Akagi, S. K., Craven, J. S., Taylor, J. W., Mcmeeking, G. R., Yokelson, R. J., Burling, I. R., Urbanski, S. P., Wold, C. E.,
10 Seinfeld, J. H., Coe, H., Alvarado, M. J. and Weise, D. R.: Evolution of trace gases and particles emitted by a
11 chaparral fire in California, *Atmos. Chem. Phys.*, 12, 1397–1421, 2012.
- 12 Albrecht, B. A.: Aerosols, cloud microphysics, and fractional cloudiness, *Science*, 245(4923), 1227–1230, 1989.
- 13 Alfarra, M. R., Coe, H., Allan, J. D., Bower, K. N., Boudries, H., Canagaratna, M. R., Jimenez, J. L., Jayne, J. T., Garforth,
14 A. A., Li, S.-M. and Worsnop, D. R.: Characterization of urban and rural organic particulate in the Lower Fraser
15 Valley using two Aerodyne Aerosol Mass Spectrometers, *Atmos. Environ.*, 38(34), 5745–5758, 2004.
- 16 Andela, N., Morton, D. C., Giglio, L., Paugam, R., Chen, Y., Hantson, S., Werf, G. R. and Randerson, J. T.: The Global Fire
17 Atlas of individual fire size, duration, speed and direction, *Earth System Science Data*, 11(2), 529–552, 2019.
- 18 Andreae, M. O.: Emission of trace gases and aerosols from biomass burning – an updated assessment,
19 *Atmos. Chem. Phys.*, 19, 8523–8546, <https://doi.org/10.5194/acp-19-8523-2019>, 2019.
- 20 Badosa, J., Wood, J., Blanc, P., Long, C. N., Vuilleumier, L., Demengel, D. and Haefelin, M.: Solar irradiances measured
21 using SPN1 radiometers: uncertainties and clues for development, *Atmospheric Measurement Techniques*, 7, 4267–
22 4283, 2014.

- 23 Bian, Q., Jathar, S. H., Kodros, J. K., Barsanti, K. C., Hatch, L. E., May, A. A., Kreidenweis, S. M. and Pierce, J. R.:
24 Secondary organic aerosol formation in biomass-burning plumes: Theoretical analysis of lab studies and ambient
25 plumes, *Atmos. Chem. Phys.*, 17(8), 5459–5475, 2017.
- 26 Brito, J., Rizzo, L. V., Morgan, W. T., Coe, H., Johnson, B., Haywood, J., Longo, K., Freitas, S., Andreae, M. O. and
27 Artaxo, P.: Ground-based aerosol characterization during the South American Biomass Burning Analysis
28 (SAMBBA) field experiment, *Atmospheric Chemistry and Physics*, 14(22), 12069–12083, doi:10.5194/acp-14-
29 12069-2014, 2014.
- 30 Cachier, H., Liousse, C., Buat-Menard, P. and Gaudichet, A.: Particulate content of savanna fire emissions, *J. Atmos. Chem.*,
31 22(1-2), 123–148, 1995.
- 32 Canagaratna, M. R., Jimenez, J. L., Kroll, J. H., Chen, Q., Kessler, S. H., Massoli, P., Hildebrandt Ruiz, L., Fortner, E.,
33 Williams, L. R., Wilson, K. R. and Others: Elemental ratios measurements of organic compounds using aerosol
34 mass spectrometry: characterization, improved calibration, and implications, *Atmos. Chem. Phys.*, 15, 253–272,
35 2015.
- 36 Capes, G., Johnson, B., McFiggans, G., Williams, P. I., Haywood, J. and Coe, H.: Aging of biomass burning aerosols over
37 West Africa: Aircraft measurements of chemical composition, microphysical properties, and emission ratios, *J.*
38 *Geophys. Res. D: Atmos.*, 113(23), 0–15, 2008.
- 39 Cappa, C. D. and Jimenez, J. L.: Quantitative estimates of the volatility of ambient organic aerosol, *Atmos. Chem. Phys.*,
40 10(12), 5409–5424, 2010.
- 41 Cappa, C. D. and Wilson, K. R.: Multi-generation gas-phase oxidation, equilibrium partitioning, and the formation and
42 evolution of secondary organic aerosol, *Atmos. Chem. Phys.*, 12(20), 9505–9528, 2012.
- 43 Carrico, C. M., Petters, M. D., Kreidenweis, S. M., Collett, J. L., Jr., Engling, G. and Malm, W. C.: Aerosol hygroscopicity
44 and cloud droplet activation of extracts of filters from biomass burning experiments, *J. Geophys. Res.*, 113(D8),
45 4767, 2008.
- 46 Canagaratna, M., Jayne, J., Jimenez, J., Allan, J., Alfarra, M., Zhang, Q., Onasch, T., Drewnick, F., Coe, H., Middlebrook,
47 A., Delia, A., Williams, L., Trimborn, A., Northway, M., DeCarlo, P., Kolb, C., Davidovits, P. and Worsnop, D.:
48 Chemical and microphysical characterization of ambient aerosols with the aerodyne aerosol mass spectrometer,
49 *Mass Spectrom. Rev.*, 26: 185-222. doi:10.1002/mas.20115, 2007

- 55 Chen, Q., Heald, C. L., Jimenez, J. L., Canagaratna, M. R., Qi, Z., Ling-Yan, H., Xiao-Feng, H., Campuzano-Jost, P., Palm,
56 B. B., Poulain, L., Kuwata, M., Martin, S. T., Ab-batt, J. P. D., Lee, A. K. Y., and Liggio, J.: Elemental
57 composition of organic aerosol: the gap between ambient and laboratory measurements, *Geophysical Research*
58 *Letters*, 42, 4182-4189, <https://doi.org/10.1002/2015gl063693>, 2015
- 59 Collier, S., Zhou, S., Onasch, T. B., Jaffe, D. A., Kleinman, L., Sedlacek, A. J., Briggs, N. L., Hee, J., Fortner, E., Shilling, J.
60 E., Worsnop, D., Yokelson, R. J., Parworth, C., Ge, X., Xu, J., Butterfield, Z., Chand, D., Dubey, M. K., Pekour, M.
61 S., Springston, S. and Zhang, Q.: Regional Influence of Aerosol Emissions from Wildfires Driven by Combustion
62 Efficiency: Insights from the BBOP Campaign, *Environmental Science and Technology*, 50(16), 8613–8622, 2016.
- 63 Collier, S., Williams, L. R., Onasch, T. B., Cappa, C. D., Zhang, X., Russell, L. M., Chen, C. L., Sanchez, K. J., Worsnop,
64 D. R. and Zhang, Q.: Influence of Emissions and Aqueous Processing on Particles Containing Black Carbon in a
65 Polluted Urban Environment: Insights From a Soot Particle-Aerosol Mass Spectrometer, *J. Geophys. Res. Atmos.*,
66 123(12), 6648–6666, doi:10.1002/2017JD027851, 2018.
- 67 Corbin, J. C., Lohmann, U., Sierau, B., Keller, A., Burtscher, H., and Mensah, A. A.: Black carbon surface oxidation and
68 organic composition of beech-wood soot aerosols, *Atmos. Chem. Phys.*, 15, 11885–11907,
69 <https://doi.org/10.5194/acp-15-11885-2015>, 2015.
- 70 Cubison, M. J., Ortega, A. M., Hayes, P. L., Farmer, D. K., Day, D., Lechner, M. J., Brune, W. H., Apel, E., Diskin, G. S.,
71 Fisher, J. A., Fuelberg, H. E., Hecobian, A., Knapp, D. J., Mikoviny, T., Riemer, D., Sachse, G. W., Sessions, W.,
72 Weber, R. J., Weinheimer, A. J., Wisthaler, A. and Jimenez, J. L.: Effects of aging on organic aerosol from open
73 biomass burning smoke in aircraft and laboratory studies, *Atmos. Chem. Phys.*, 11(23), 12049–12064, 2011.
- 74 Dal Maso, M., Kulmala, M., Lehtinen, K. E. J., Mäkelä, J. M., Aalto, P., and O'Dowd, C. D.: Condensation and coagulation
75 sinks and formation of nucleation mode particles in coastal and boreal forest boundary layers, *J. Geophys. Res.*,
76 107(D19), doi:[10.1029/2001JD001053](https://doi.org/10.1029/2001JD001053), 2002.
- 77 Decarlo, P. F., Dunlea, E. J., Kimmel, J. R., Aiken, A. C., Sueper, D., Crouse, J., Wennberg, P. O., Emmons, L., Shinozuka,
78 Y., Clarke, A., Zhou, J., Tomlinson, J., Collins, D. R., Knapp, D., Weinheimer, A. J., Montzka, D. D., Campos, T.
79 and Jimenez, J. L.: Fast airborne aerosol size and chemistry measurements above Mexico City and Central Mexico
80 during the MILAGRO campaign., 2008.
- 81 Dennison, P. E., Brewer, S. C., Arnold, J. D. and Moritz, M. A.: Large wildfire trends in the western United States, 1984-
82 2011, *Geophysical Research Letters*, 41(8), 2928–2933, doi:10.1002/2014gl059576, 2014.
- 83 Eatough, D. J., Eatough, N. L., Pang, Y., Sizemore, S., Kirchstetter, T. W., Novakov, T. and Hobbs, P. V.: Semivolatile
84 particulate organic material in southern Africa during SAFARI 2000, *J. Geophys. Res. D: Atmos.*, 108(D13)
85 [online] Available from:
86 [https://agupubs.onlinelibrary.wiley.com/doi/abs/10.1029/2002JD002296%4010.1002/%28ISSN%292169-](https://agupubs.onlinelibrary.wiley.com/doi/abs/10.1029/2002JD002296%4010.1002/%28ISSN%292169-8996.SAF1)
87 [8996.SAF1](https://agupubs.onlinelibrary.wiley.com/doi/abs/10.1029/2002JD002296%4010.1002/%28ISSN%292169-8996.SAF1), 2003.
- 88 Evans, J. D. (1996). *Straightforward statistics for the behavioral sciences*. Thomson Brooks/Cole Publishing Co.

- 89 Ford, B., Val Martin, M., Zelasky, S. E., Fischer, E. V., Anenberg, S. C., Heald, C. L. and Pierce, J. R.: Future Fire Impacts
90 on Smoke Concentrations, Visibility, and Health in the Contiguous United States, *GeoHealth*,
91 doi:10.1029/2018GH000144, 2018.
- 92 Formenti, P., Elbert, W., Maenhaut, W., Haywood, J., Osborne, S. and Andreae, M. O.: Inorganic and carbonaceous aerosols
93 during the Southern African Regional Science Initiative (SAFARI 2000) experiment: Chemical characteristics,
94 physical properties, and emission data for smoke from African biomass burning, *J. Geophys. Res. D: Atmos.*,
95 108(D13), doi:10.1029/2002JD002408, 2003.
- 96 Forrister, H., Liu, J., Scheuer, E., Dibb, J., Ziemba, L., Thornhill, K. L., Anderson, B., Diskin, G., Perring, A. E., Schwarz, J.
97 P., Campuzano-Jost, P., Day, D. A., Palm, B. B., Jimenez, J. L., Nenes, A. and Weber, R. J.: Evolution of brown
98 carbon in wildfire plumes, *Geophys. Res. Lett.*, 42(11), 4623–4630, 2015.
- 99 Gan, R. W., Ford, B., Lassman, W., Pfister, G., Vaidyanathan, A., Fischer, E., Volckens, J., Pierce, J. R. and Magzamen, S.:
00 Comparison of wildfire smoke estimation methods and associations with cardiopulmonary-related hospital
01 admissions, *GeoHealth*, 1(3), 122–136, 2017.
- 02 Garofalo, L., Pothier, M. A., Levin, E. J. T., Campos, T., Kreidenweis, S. M. and Farmer, D. K.: Emission and Evolution of
03 Submicron Organic Aerosol in Smoke from Wildfires in the Western United States, *ACS Earth and Space*
04 *Chemistry*, acsearthspacechem.9b00125, 2019.
- 05 Giglio, L., Csiszar, I. and Justice, C. O.: Global distribution and seasonality of active fires as observed with the Terra and
06 Aqua Moderate Resolution Imaging Spectroradiometer (MODIS) sensors, *Journal of Geophysical Research:*
07 *Biogeosciences*, 111(G2) [online] Available from:
08 <https://agupubs.onlinelibrary.wiley.com/doi/abs/10.1029/2005JG000142>, 2006.
- 09 Giglio, L., Csiszar, I., Restás, Á., Morisette, J. T., Schroeder, W., Morton, D. and Justice, C. O.: Active fire detection and
10 characterization with the advanced spaceborne thermal emission and reflection radiometer (ASTER), *Remote*
11 *Sensing of Environment*, 112(6), 3055–3063, doi:10.1016/j.rse.2008.03.003, 2008.
- 12 Gilman, J. B., Lerner, B. M., Kuster, W. C., Goldan, P. D., Warneke, C., Veres, P. R., Roberts, J. M., De Gouw, J. A.,
13 Burling, I. R. and Yokelson, R. J.: Biomass burning emissions and potential air quality impacts of volatile organic
14 compounds and other trace gases from fuels common in the US, *Atmos. Chem. Phys.*, 15(24), 13915–13938, 2015.
- 15 Grieshop, A. P., Logue, J. M., Donahue, N. M., and Robinson, A. L.: Laboratory investigation of photochemical oxidation of
16 organic aerosol from wood fires 1: measurement and simulation of organic aerosol evolution, *Atmos. Chem. Phys.*,
17 9, 1263–1277, <https://doi.org/10.5194/acp-9-1263-2009>, 2009.
- 18 Hatch, L. E., Luo, W., Pankow, J. F., Yokelson, R. J., Stockwell, C. E. and Barsanti, K. C.: Identification and quantification
19 of gaseous organic compounds emitted from biomass burning using two-dimensional gas chromatography-time-of-
20 flight mass spectrometry, *Atmos. Chem. Phys.*, 15(4), 1865–1899, 2015.

21 Hatch, L. E., Yokelson, R. J., Stockwell, C. E., Veres, P. R., Simpson, I. J., Blake, D. R., Orlando, J. J. and Barsanti, K. C.:
22 Multi-instrument comparison and compilation of non-methane organic gas emissions from biomass burning and
23 implications for smoke-derived secondary organic aerosol precursors, *Atmos. Chem. Phys.*, 17, 1471–1489, 2017.

24 Heald, C. L., Kroll, J. H., Jimenez, J. L., Docherty, K. S., DeCarlo, P. F., Aiken, A. C., Chen, Q., Martin, S. T., Farmer, D.
25 K. and Artaxo, P.: A simplified description of the evolution of organic aerosol composition in the atmosphere,
26 *Geophys. Res. Lett.*, 37(8), doi:10.1029/2010GL042737, 2010.

27 Hecobian, A., Liu, Z., Hennigan, C. J., Huey, L. G., Jimenez, J. L., Cubison, M. J., Vay, S., Diskin, G. S., Sachse, G. W.,
28 Wisthaler, A., Mikoviny, T., Weinheimer, A. J., Liao, J., Knapp, D. J., Wennberg, P. O., Urten, A., Crouse, J. D.,
29 Clair, J. S., Wang, Y. and Weber, R. J.: Comparison of chemical characteristics of 495 biomass burning plumes
30 intercepted by the NASA DC-8 aircraft during the ARCTAS/CARB-2008 field campaign, *Atmos. Chem. Phys.*, 11,
31 13325–13337, 2011.

32 Hennigan, C. J., Miracolo, M. A., Engelhart, G. J., May, A. A., Presto, A. A., Lee, T., Sullivan, A. P., McMeeking, G. R.,
33 Coe, H., Wold, C. E., Hao, W. M., Gilman, J. B., Kuster, W. C., De Gouw, J., Schichtel, B. A., Collett, J. L.,
34 Kreidenweis, S. M. and Robinson, A. L.: Chemical and physical transformations of organic aerosol from the photo-
35 oxidation of open biomass burning emissions in an environmental chamber, *Atmos. Chem. Phys.*, 11(15), 7669–
36 7686, doi:10.5194/acp-11-7669-2011, 2011.

37 Hobbs, P. V., Sinha, P., Yokelson, R. J., Christian, T. J., Blake, D. R., Gao, S., Kirchstetter, T. W., Novakov, T. and
38 Pilewskie, P.: Evolution of gases and particles from a savanna fire in South Africa, *J. Geophys. Res. D: Atmos.*,
39 108(D13), doi:10.1029/2002JD002352, 2003.

40 Hodshire, A. L., Akherati, A., Alvarado, M. J., Brown-Steiner, B., Jathar, S. H., Jimenez, J. L., Kreidenweis, S. M.,
41 Lonsdale, C. R., Onasch, T. B., Ortega, A. M. and Pierce, J. R.: Aging Effects on Biomass Burning Aerosol Mass
42 and Composition: A Critical Review of Field and Laboratory Studies, *Environ. Sci. Technol.*, 53(17), 10007–
43 10022, 2019a.

44 Hodshire, A. L., Bian, Q., Ramnarine, E., Lonsdale, C. R., Alvarado, M. J., Kreidenweis, S. M., Jathar, S. H. and Pierce, J.
45 R.: More than emissions and chemistry: Fire size, dilution, and background aerosol also greatly influence near-field
46 biomass burning aerosol aging, *J. Geophys. Res. D: Atmos.*, 2018JD029674, 2019b.

47 Huffman, J. A., Docherty, K. S., Aiken, A. C., Cubison, M. J., Ulbrich, I. M., Decarlo, P. F., Sueper, D., Jayne, J. T.,
48 Worsnop, D. R., Ziemann, P. J. and Jimenez, J. L.: Chemically-resolved aerosol volatility measurements from two
49 megacity field studies., 2009.

50 Janhäll, S., Andreae, M. O. and Pöschl, U.: Biomass burning aerosol emissions from vegetation fires: particle number and
51 mass emission factors and size distributions, *Atmos. Chem. Phys. Disc.*, 9(4), 17183–17217, 2009.

52 Jen, C. N., Hatch, L. E., Selimovic, V., Yokelson, R. J., Weber, R., Fernandez, A. E., Kreisberg, N. M., Barsanti, K. C. and
53 Goldstein, A. H.: Speciated and total emission factors of particulate organics from burning western US wildland
54 fuels and their dependence on combustion efficiency, *Atmos. Chem. Phys.*, 19, 1013–1026, 2019.

55 Jimenez, J. L., Canagaratna, M. R., Donahue, N. M., Prevot, a. S. H., Zhang, Q., Kroll, J. H., DeCarlo, P. F., Allan, J. D.,
56 Coe, H., Ng, N. L., Aiken, a. C., Docherty, K. S., Ulbrich, I. M., Grieshop, a. P., Robinson, a. L., Duplissy, J.,
57 Smith, J. D., Wilson, K. R., Lanz, V. a., Hueglin, C., Sun, Y. L., Tian, J., Laaksonen, A., Raatikainen, T.,
58 Rautiainen, J., Vaattovaara, P., Ehn, M., Kulmala, M., Tomlinson, J. M., Collins, D. R., Cubison, M. J., Dunlea, E.
59 J., Huffman, J. a., Onasch, T. B., Alfarra, M. R., Williams, P. I., Bower, K., Kondo, Y., Schneider, J., Drewnick, F.,
60 Borrmann, S., Weimer, S., Demerjian, K., Salcedo, D., Cottrell, L., Griffin, R., Takami, A., Miyoshi, T.,
61 Hatakeyama, S., Shimono, A., Sun, J. Y., Zhang, Y. M., Dzepina, K., Kimmel, J. R., Sueper, D., Jayne, J. T.,
62 Herndon, S. C., Trimborn, a. M., Williams, L. R., Wood, E. C., Middlebrook, a. M., Kolb, C. E., Baltensperger, U.
63 and Worsnop, D. R.: Evolution of organic aerosols in the atmosphere, *Science*, 326(5959), 1525–1529, 2009.

64 Jolleys, M. D., Coe, H., McFiggans, G., Capes, G., Allan, J. D., Crosier, J., Williams, P. I., Allen, G., Bower, K. N., Jimenez,
65 J. L., Russell, L. M., Grutter, M. and Baumgardner, D.: Characterizing the aging of biomass burning organic aerosol
66 by use of mixing ratios: A meta-analysis of four regions, *Environmental Science and Technology*, 46(24), 13093–
67 13102, 2012.

68 Jolleys, M. D., Coe, H., McFiggans, G., Taylor, J. W., O’Shea, S. J., Le Breton, M., Bauguitte, S. J. B., Moller, S., Di Carlo,
69 P., Aruffo, E., Palmer, P. I., Lee, J. D., Percival, C. J. and Gallagher, M. W.: Properties and evolution of biomass
70 burning organic aerosol from Canadian boreal forest fires, *Atmos. Chem. Phys.*, 15(6), 3077–3095, 2015.

71 Kleinman, L. I., Daum, P. H., Lee, Y. N., Senum, G. I., Springston, S. R., Wang, J., Berkowitz, C., Hubbe, J., Zaveri, R. A.,
72 Brechtel, F. J., Jayne, J., Onasch, T. B. and Worsnop, D.: Aircraft observations of aerosol composition and ageing
73 in New England and Mid-Atlantic States during the summer 2002 New England Air Quality Study field campaign,
74 *J. Geophys. Res. Atmos.*, 112(9), 1–18, doi:10.1029/2006JD007786, 2007.

75 Kleinman, L. and Sedlacek, A. J., III: Biomass Burning Observation Project (BBOP) Final Campaign Report, 2016.

76 Kleinman, L. I., Sedlacek, A. J., III, Adachi, K., Buseck, P. R., Collier, S., Dubey, M., K., Hodshire, A. L., Lewis, E.,
77 Onasch, T. B., Pierce, J. R., Schilling, J., Springston, S. R., Wang, J., Zhang, Q., Zhou, S., Yokelson, R. J.: Rapid
78 Evolution of Aerosol Particles and their Optical Properties Downwind of Wildfires in the Western U.S., submitted
79 to *Atmos. Chem. Phys.*, 2020.

80 Konovalov, I. B., Beekmann, M., Golovushkin, N. A. and Andreae, M. O.: Nonlinear behavior of organic aerosol in biomass
81 burning plumes: a microphysical model analysis, *Atmos. Chem. Phys. Disc.*, 1–44, 2019.

82 Koss, A. R., Sekimoto, K., Gilman, J. B., Selimovic, V., Coggon, M. M., Zarzana, K. J., Yuan, B., Lerner, B. M., Brown, S.
83 S., Jimenez, J. L., Krechmer, J., Roberts, J. M., Warneke, C., Yokelson, R. J. and De Gouw, J.: Non-methane
84 organic gas emissions from biomass burning: Identification, quantification, and emission factors from PTR-ToF
85 during the FIREX 2016 laboratory experiment, *Atmos. Chem. Phys.*, 18(5), 3299–3319, 2018.

86 Kroll, J. H. and Seinfeld, J. H.: Chemistry of secondary organic aerosol: Formation and evolution of low-volatility organics
87 in the atmosphere, *Atmos. Environ.*, 42, 3593–3624, 2008.

88 Kulkarni, P. and Wang, J.: New fast integrated mobility spectrometer for real-time measurement of aerosol size
89 distribution—I: Concept and theory, *J. Aerosol Sci.*, 37(10), 1303–1325, 2006.

90 Lee, J. E., Dubey, M. K., Aiken, A. C., Chylek, P., & Carrico, C. M.: Optical and chemical analysis of absorption
91 enhancement by mixed carbonaceous aerosols in the 2019 Woodbury, AZ fire plume, *J. Geophys. Res. Atmos.*,
92 125, e2020JD032399. <https://doi.org/10.1029/2020JD032399>, 2020.

93 Lee, T., Sullivan, A. P., Mack, L., Jimenez, J. L., Kreidenweis, S. M., Onasch, T. B., Worsnop, D. R., Malm, W., Wold, C.
94 E., Hao, W. M. and Collett, J. L.: Chemical Smoke Marker Emissions During Flaming and Smoldering Phases of
95 Laboratory Open Burning of Wildland Fuels, *Aerosol Sci. Technol.*, 44(9), i–v, 2010.

96 Lim, C. Y., Hagan, D. H., Coggon, M. M., Koss, A. R., Sekimoto, K., de Gouw, J., Warneke, C., Cappa, C. D., and Kroll, J.
97 H.: Secondary organic aerosol formation from the laboratory oxidation of biomass burning emissions, *920 Atmos.*
98 *Chem. Phys.*, 19, 12797-12809, 10.5194/acp-19-12797-2019, 2019.

99 Liu, X., Zhang, Y., Huey, L. G., Yokelson, R. J., Wang, Y., Jimenez, J. L., Campuzano-Jost, P., Beyersdorf, A. J., Blake, D.
00 R., Choi, Y., St. Clair, J. M., Crounse, J. D., Day, D. A., Diskin, G. S., Ried, A., Hall, S. R., Hanisco, T. F., King, L.
01 E., Meinardi, S., Mikoviny, T., Palm, B. B., Peischl, J., Perring, A. E., Pollack, I. B., Ryerson, T. B., Sachse, G.,
02 Schwarz, J. P., Simpson, I. J., Tanner, D. J., Thornhil, K. L., Ullmann, K., Weber, R. J., Wennberg, P. O.,
03 Wisthaler, A., Wolfe, G. M. and Ziemba, L. D.: Agricultural fires in the southeastern U.S. during SEAC4RS:
04 Emissions of trace gases and particles and evolution of ozone, reactive nitrogen, and organic aerosol, *J. Geophys.*
05 *Res.*, 121(12), 7383–7414, 2016.

06 Liu, P.S.K., Deng, R., Smith, K.A., Williams, L.R., Jayne, J.T., Canagaratna, M.R., Moore, K., Onasch, T.B., Worsnop,
07 D.R., and Deshler, T.: Transmission Efficiency of an Aerodynamic Focusing Lens System: Comparison of Model
08 Calculations and Laboratory Measurements for the Aerodyne Aerosol Mass Spectrometer, *Aerosol Sci. Technol.*,
09 41(8):721–733, 2007Long, C. N., Bucholtz, A., Jonsson, H., Schmid, B., Vogelmann, A. and Wood, J.: A Method
10 of Correcting for Tilt from Horizontal in Downwelling Shortwave Irradiance Measurements on Moving Platforms,
11 *The Open Atmospheric Science Journal*, 4(1), 78–87, doi:10.2174/1874282301004010078, 2010.

12 Massoli, P., Onasch, T. B., Cappa, C. D., Nuamaan, I., Hakala, J., Hayden, K., Li, S., Sueper, D. T., Bates, T. S., Quinn, P.
13 K., Jayne, J. T., and Worsnop, D. R.: Characterization of black carbon-containing particles from soot particle
14 aerosol mass spectrometer measurements on the R/V Atlantis during CalNex 2010. *J. Geophys. Res. Atmos.*, 120,
15 2575– 2593. doi: 10.1002/2014JD022834, 2015.

16 May, A. A., Levin, E. J. T., Hennigan, C. J., Riipinen, I., Lee, T., Collett, J. L., Jimenez, J. L., Kreidenweis, S. M. and
17 Robinson, A. L.: Gas-particle partitioning of primary organic aerosol emissions: 3. Biomass burning, *J. Geophys.*
18 *Res. D: Atmos.*, 118(19), 11327–11338, 2013.

19 May, A. A., Lee, T., McMeeking, G. R., Akagi, S., Sullivan, A. P., Urbanski, S., Yokelson, R. J. and Kreidenweis, S. M.:
20 Observations and analysis of organic aerosol evolution in some prescribed fire smoke plumes, *Atmos. Chem. Phys.*,
21 15(11), 6323–6335, 2015.

- 22 McClure, C. D., Lim, C. Y., Hagan, D. H., Kroll, J. H., and Cappa, C. D.: Biomass-burning-derived particles from a wide
23 variety of fuels – Part 1: Properties of primary particles, *Atmos. Chem. Phys.*, 20, 1531-1547,
24 <https://doi.org/10.5194/acp-20-1531-2020>, 2020.
- 25 Middlebrook, A. M., Bahreini, R., Jimenez, J. L. and Canagaratna, M. R.: Evaluation of composition-dependent collection
26 efficiencies for the Aerodyne aerosol mass spectrometer using field data, *Aerosol Sci. Technol.*, 46(3), 258–271,
27 doi:10.1080/02786826.2011.620041, 2012.
- 28 Morgan, W. T., Allan, J. D., Bauguitte, S., Darbyshire, E., Flynn, M. J., Lee, J., Liu, D., Johnson, B., Haywood, J., Longo,
29 K. M., Artaxo, P. E. and Coe, H.: Transformation and aging of biomass burning carbonaceous aerosol over tropical
30 South America from aircraft in-situ measurements during SAMBBA, *Atmos. Chem. Phys. Discuss.*,
31 doi:10.5194/acp-2019-157, 2019.
- 32 Moteki, N. and Kondo, Y.: Dependence of Laser-Induced Incandescence on Physical Properties of Black Carbon Aerosols:
33 Measurements and Theoretical Interpretation, *Aerosol Sci. Technol.*, 44(8), 663–675, 2010.
- 34 Nance, J. D., Hobbs, P. V. and Radkel, L. F.: Airborne Measurements of Gases and Particles From an Alaskan Wildfire, *J.*
35 *Geophys. Res. D: Atmos.*, 98(D8), 873–882, 1993.
- 36 Noyes, K. J., Kahn, R., Sedlacek, A., Kleinman, L., Limbacher, J. and Li, Z.: Wildfire Smoke Particle Properties and
37 Evolution, from Space-Based Multi-Angle Imaging, *Remote Sensing*, 12(5), 769, doi:10.3390/rs12050769, 2020.
- 38 O’Dell, K., Ford, B., Fischer, E. V. and Pierce, J. R.: Contribution of Wildland-Fire Smoke to US PM_{2.5} and Its Influence
39 on Recent Trends, *Environmental Science & Technology*, 53(4), 1797–1804, doi:10.1021/acs.est.8b05430, 2019.
- 40 Olfert, J. S. and Wang, J.: Dynamic Characteristics of a Fast-Response Aerosol Size Spectrometer, *Aerosol Sci. Technol.*,
41 43(2), 97–111, 2009.
- 42 Onasch, T. B., Trimborn, A., Fortner, E. C., Jayne, J. T., Kok, G. L., Williams, L. R., Davidovits, P. and Worsnop, D. R.:
43 Soot Particle Aerosol Mass Spectrometer: Development, Validation, and Initial Application, *Aerosol Science and*
44 *Technology*, 46(7), 804–817, doi:10.1080/02786826.2012.663948, 2012.
- 45 Palm, B. B., Peng, Q., Fredrickson, C. D., Lee, B. H., Garofalo, L. A. and Pothier, M. A.: Quantification of organic aerosol
46 and brown carbon evolution in fresh wildfire plumes, , doi:10.1073/pnas.2012218117, 2020.
- 47 Petters, M. D. and Kreidenweis, S. M.: A single parameter representation of hygroscopic growth and cloud condensation
48 nucleus activity, *Atmos. Chem. Phys.*, 7(8), 1961–1971, 2007.
- 49 Petters, M. D., Carrico, C. M., Kreidenweis, S. M., Prenni, A. J., DeMott, P. J., Collett, J. L. and Moosmüller, H.: Cloud
50 condensation nucleation activity of biomass burning aerosol, *J. Geophys. Res. D: Atmos.*, 114(22), 22205, 2009.
- 51 Ramnarine, E., Kodros, J. K., Hodshire, A. L., Lonsdale, C. R., Alvarado, M. J. and Pierce, J. R.: Effects of near-source
52 coagulation of biomass burning aerosols on global predictions of aerosol size distributions and implications for
53 aerosol radiative effects, *Atmos. Chem. Phys.*, 19(9), 6561–6577, 2019.
- 54 Reid, C. E., Brauer, M., Johnston, F. H., Jerrett, M., Balmes, J. R. and Elliott, C. T.: Critical review of health impacts of
55 wildfire smoke exposure, *Environmental Health Perspectives*, 124(9), 1334–1343, doi:10.1289/ehp.1409277, 2016.

56 Reid, J. S., Hobbs, P. V., Ferek, R. J., Blake, D. R., Martins, J. V., Dunlap, M. R. and Liousse, C.: Physical, chemical, and
57 optical properties of regional hazes dominated by smoke in Brazil, *J. Geophys. Res. D: Atmos.*, 103(D24), 32059–
58 32080, 1998.

59 Reid, J. S., Eck, T. F., Christopher, S. A., Koppmann, R., Dubovik, O., Eleuterio, D. P., Holben, B. N., Reid, E. A. and
60 Zhang, J.: A review of biomass burning emissions part III: intensive optical properties of biomass burning particles,
61 *Atmos. Chem. Phys.*, 5, 827–849, 2005.

62 Sakamoto, K. M., Allan, J. D., Coe, H., Taylor, J. W., Duck, T. J. and Pierce, J. R.: Aged boreal biomass-burning aerosol
63 size distributions from BORTAS 2011, *Atmos. Chem. Phys.*, 15(4), 1633–1646, 2015.

64 Sakamoto, K. M., Laing, J. R., Stevens, R. G., Jaffe, D. A. and Pierce, J. R.: The evolution of biomass-burning aerosol size
65 distributions due to coagulation: Dependence on fire and meteorological details and parameterization, *Atmos.*
66 *Chem. Phys.*, 16(12), 7709–7724, 2016.

67 Schwarz, J. P., Gao, R. S., Fahey, D. W., Thomson, D. S., Watts, L. A., Wilson, J. C., Reeves, J. M., Darbeheshti, M.,
68 Baumgardner, D. G., Kok, G. L. and Others: Single-particle measurements of midlatitude black carbon and light-
69 scattering aerosols from the boundary layer to the lower stratosphere, *J. Geophys. Res. D: Atmos.*, 111(D16)
70 [online] Available from: <https://agupubs.onlinelibrary.wiley.com/doi/abs/10.1029/2006JD007076>, 2006.

71 Schwarz, J.P., Spackman, J.R., Gao, R.S., Perring, a. E., Cross, E., Onasch, T.B., Ahern, a., Wrobel, W., Davidovits, P.,
72 Olfert, J., Dubey, M.K., Mazzoleni, C., and Fahey, D.W.: The Detection Efficiency of the Single Particle Soot
73 Photometer, *Aerosol Sci. Technol.*, 44(8):612–628, 2010. Sedlacek, A. J., Iii, Buseck, P. R., Adachi, K., Onasch, T.
74 B., Springston, S. R. and Kleinman, L.: Formation and evolution of Tar Balls from Northwestern US wildfires,
75 *Atmos. Chem. Phys. Discuss.*, (Figure 1), 1–28, 2018.

76 Seinfeld, J. H. and Pandis, S. N.: *Atmospheric chemistry and physics: From air pollution to climate change*, John Willey &
77 Sons, Inc. , New York, 2006.

78

79 Shrivastava, M., Cappa, C. D., Fan, J., Goldstein, A. H., Guenther, A. B., Jimenez, J. L., Kuang, C., Laskin, A., Martin, S.
80 T., Ng, N. L. and Others: Recent advances in understanding secondary organic aerosol: Implications for global
81 climate forcing, *Rev. Geophys.*, 55(2), 509–559, 2017.

82 Spracklen, D. V., Mickley, L. J., Logan, J. A., Hudman, R. C., Yevich, R., Flannigan, M. D. and Westerling, A. L.: Impacts
83 of climate change from 2000 to 2050 on wildfire activity and carbonaceous aerosol concentrations in the western
84 United States, *J. Geophys. Res.*, 114(D20), 1418, 2009.

85 Tang, X., Madronich, S., Wallington, T. and Calamari, D.: Changes in tropospheric composition and air quality, *J.*
86 *Photochem. Photobiol. B*, 46(1-3), 83–95, 1998.

87 Tie, X.: Effect of clouds on photolysis and oxidants in the troposphere, *J. Geophys. Res.*, 108(D20), 23,073, 2003.

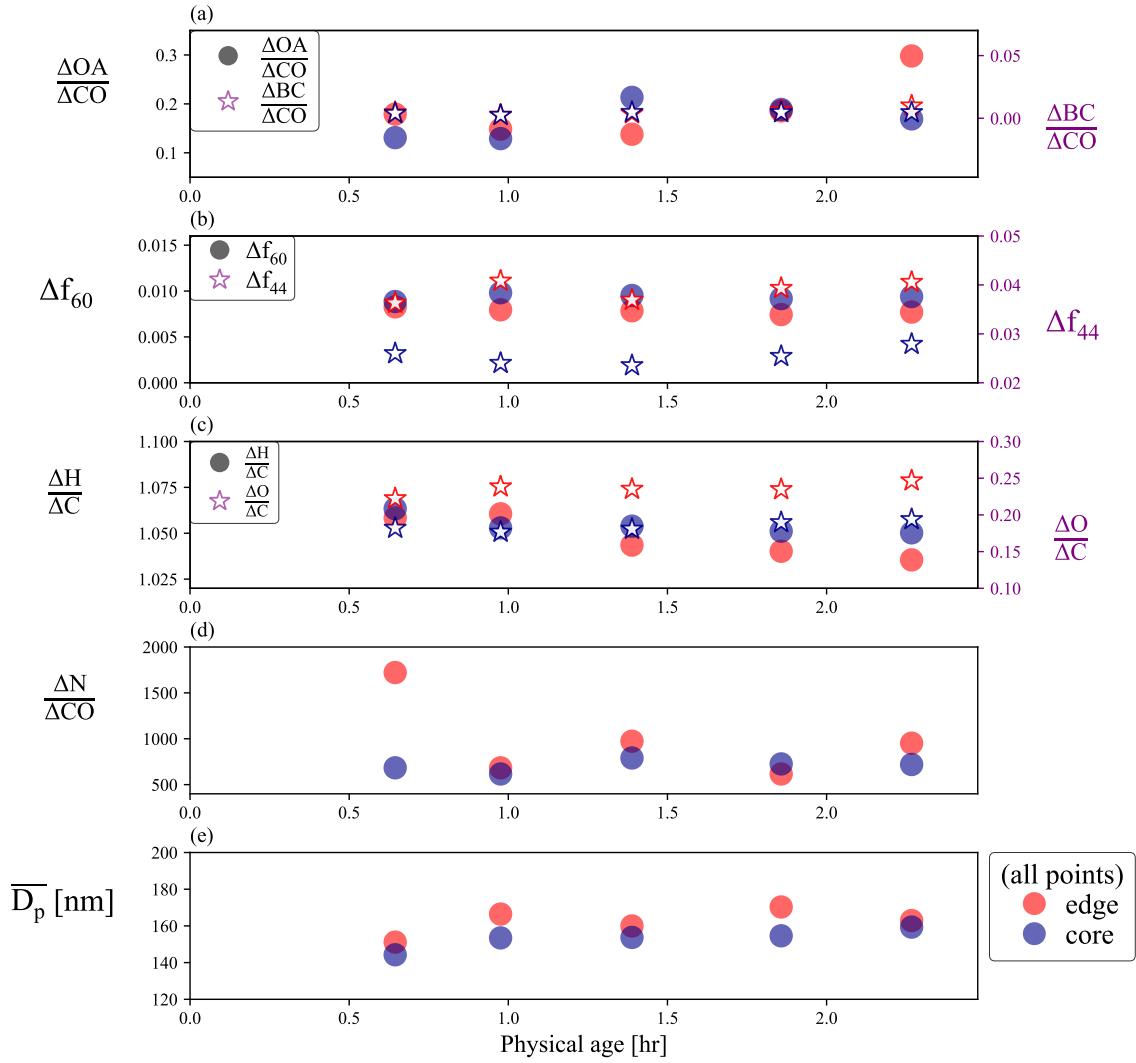
88 Twomey, S.: Pollution and the planetary albedo, *Atmos. Environ.*, 8(12), 1251–1256, 1974.

- 89 Vakkari, V., Kerminen, V.-M., Beukes, J. P., Titta, P., van Zyl, P. G., Josipovic, M., Wnter, A. D., Jaars, K., Worsnop, D.
90 R., Kulmala, M. and Laakso, L.: Rapid changes in biomass burning aerosols by atmospheric oxidation, *Geophys.*
91 *Res. Lett.*, 2644–2651, 2014.
- 92 Vakkari, V., Beukes, J. P., Dal Maso, M., Aurela, M., Josipovic, M. and van Zyl, P. G.: Major secondary aerosol formation
93 in southern African open biomass burning plumes, *Nat. Geosci.*, 11(8), 580–583, 2018.
- 94 Volkamer, R., Jimenez, J. L., San Martini, F., Dzepina, K., Zhang, Q., Salcedo, D., Molina, L. T., Worsnop, D. R. and
95 Molina, M. J.: Secondary organic aerosol formation from anthropogenic air pollution: Rapid and higher than
96 expected, *Geophys. Res. Lett.*, 33(17), 4407, 2006.
- 97 Volkamer, R., Ziemann, P. J. and Molina, M. J.: Secondary Organic Aerosol Formation from Acetylene (C₂H₂): seed effect
98 on SOA yields due to organic photochemistry in the aerosol aqueous phase, *Atmos. Chem. Phys.*, 9(6), 1907–1928,
99 2009.
- 00 Wang, J., -N. Lee, Y., Daum, P. H., Jayne, J. and Alexander, M. L.: Effects of aerosol organics on cloud condensation
01 nucleus (CCN) concentration and first indirect aerosol effect, *Atmospheric Chemistry and Physics*, 8(21), 6325–
02 6339, doi:10.5194/acp-8-6325-2008, 2008.
- 03 Willis, M. D., Lee, A. K. Y., Onasch, T. B., Fortner, E. C., Williams, L. R., Lambe, A. T., Worsnop, D. R., and Abbatt, J. P.
04 D.: Collection efficiency of the soot-particle aerosol mass spectrometer (SP-AMS) for internally mixed particulate
05 black carbon, *Atmos. Meas. Tech.*, 7, 4507–4516, <https://doi.org/10.5194/amt-7-4507-2014>, 2014.
- 06 Yang, M., Blomquist, B. W. and Huebert, B. J.: Constraining the concentration of the hydroxyl radical in a stratocumulus-
07 topped marine boundary layer from sea-to-air eddy covariance flux measurements of dimethylsulfide, *Atmos.*
08 *Chem. Phys.*, 9(23), 9225–9236, 2009.
- 09 Yokelson, R. J., Crounse, J. D., DeCarlo, P. F., Karl, T., Urbanski, S., Atlas, E., Campos, T., Shinozuka, Y., Kapustin, V.,
10 Clarke, A. D., Weinheimer, A., Knapp, D. J., Montzka, D. D., Holloway, J., Weibring, P., Flocke, F., Zheng, W.,
11 Toohey, D., Wennberg, P. O., Wiedinmyer, C., Mauldin, L., Fried, A., Richter, D., Walega, J., Jimenez, J. L.,
12 Adachi, K., Buseck, P. R., Hall, S. R. and Shetter, R.: Emissions from biomass burning in the Yucatan, *Atmos.*
13 *Chem. Phys.*, 9(15), 5785–5812, 2009.
- 14 Yue, X., Mickley, L. J., Logan, J. A. and Kaplan, J. O.: Ensemble projections of wildfire activity and carbonaceous aerosol
15 concentrations over the western United States in the mid-21st century, *Atmospheric Environment*, 77, 767–780,
16 doi:10.1016/j.atmosenv.2013.06.003, 2013.
- 17 Zhou, S., Collier, S., Jaffé, D. A., Briggs, N. L., Hee, J., Sedlacek, A. J., III, Kleinman, L., Onasch, T. B. and Zhang, Q.:
18 Regional influence of wildfires on aerosol chemistry in the western US and insights into atmospheric aging of
19 biomass burning organic aerosol, *Atmos. Chem. Phys.*, 17(3), 2477–2493, 2017.
- 20
21
22
23

24

25

26



27

28

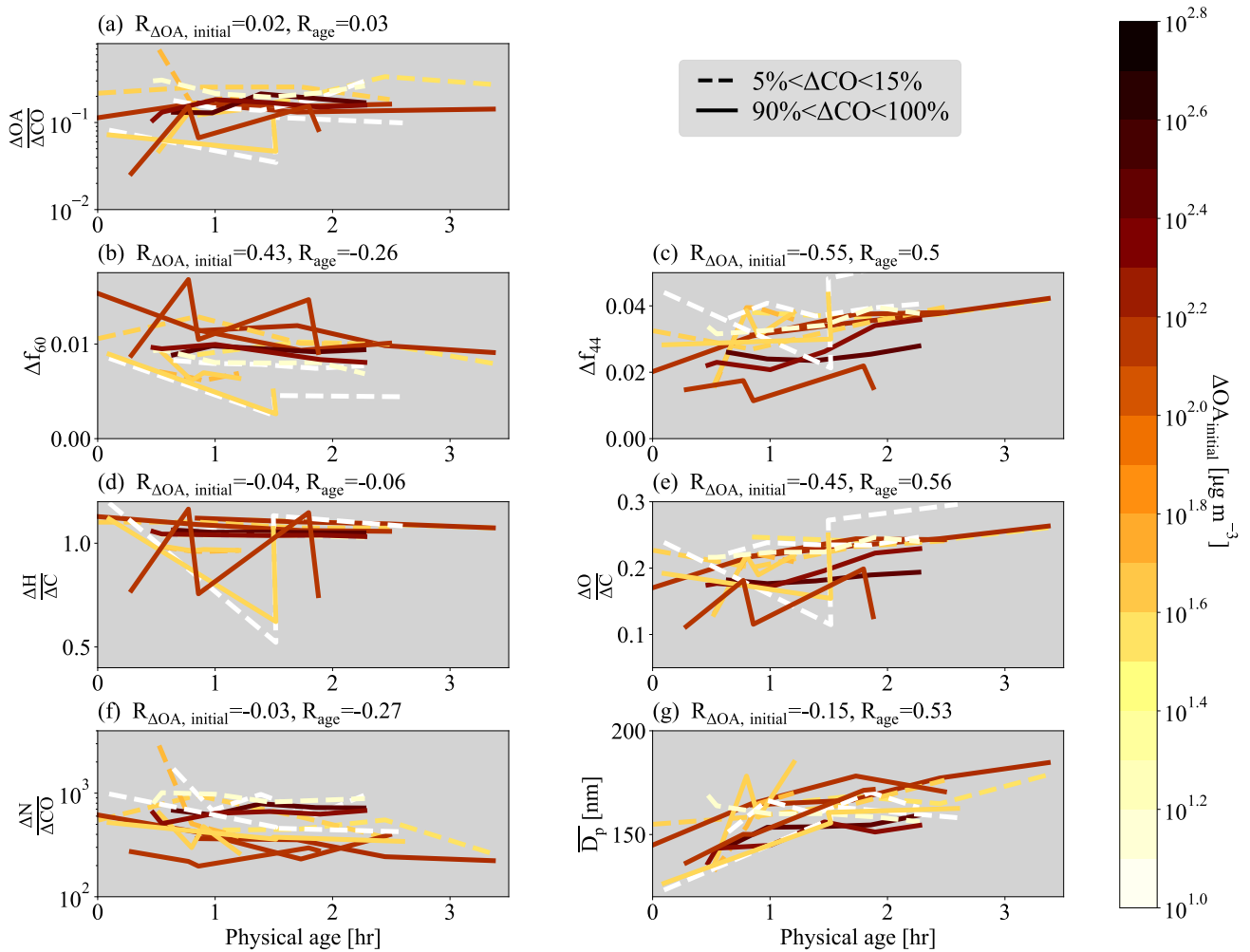
29

30

31

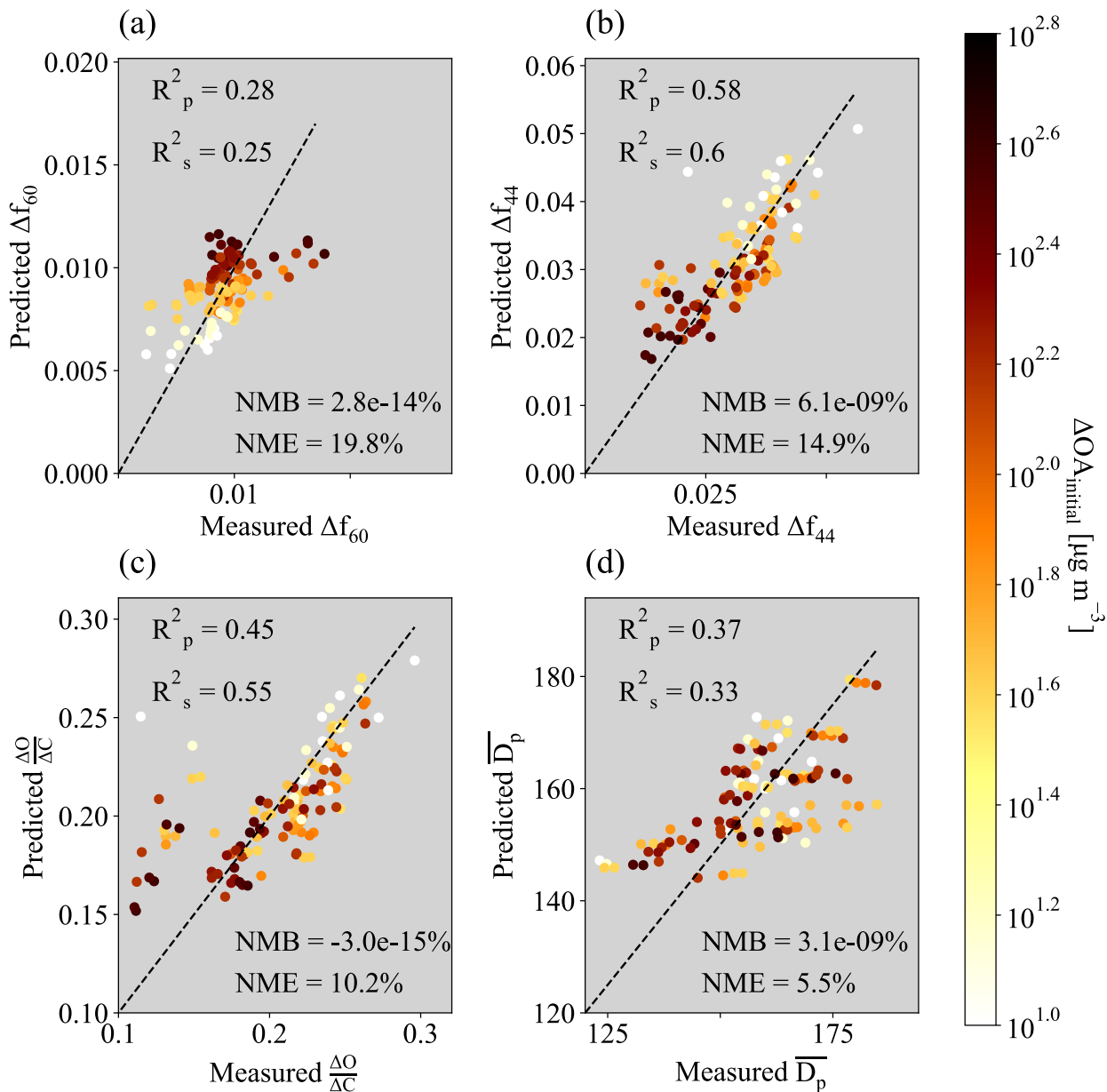
Figure 1: Aerosol properties from the first set of pseudo-Lagrangian transects from the Colockum fire on flight '730b' (a) $\Delta OA/\Delta CO$ (right y-axis) and $\Delta BC/\Delta CO$ (left y-axis), (b) Δf_{60} (right y-axis) and Δf_{44} (left y-axis), (c) $\Delta H/\Delta C$ (right y-axis) and $\Delta O/\Delta C$ (left y-axis), (d) $\Delta N/\Delta CO$, and (e) $\overline{D_p}$ against physical age. For each transect, the data is divided into edge (the lowest 5-15% of ΔCO data; red points) and core (90-100% of ΔCO data; blue points).

32



33
34
35
36
37
38
39
40
41
42
43

Figure 2. Various normalized parameters as a function of physical age for the 7 sets of pseudo-Lagrangian transects. Separate lines are shown for the edges (lowest 5-15% of ΔCO ; dashed lines) and cores (highest 90-100% of ΔCO ; solid lines). (a) $\Delta OA / \Delta CO$, (b) Δf_{60} , (c) Δf_{44} , (d) $\Delta H / \Delta C$, (e) $\Delta O / \Delta C$, (f) $\Delta N / \Delta CO$, and (g) \overline{D}_p between 40-262 nm against physical age for all flights, colored by $\Delta OA_{initial}$. Some flights have missing data. Also provided is the Spearman correlation coefficient, R , between each variable and $\Delta OA_{initial}$ and physical age for each variable. Note that panels (a) and (f) have a log y-axis.



44
45
46
47
48
49
50
51

Figure 3. Measured versus predicted (a) Δf_{60} , (b) Δf_{44} , (c) $\Delta O/\Delta C$, and (d) \overline{D}_p between 40-262 nm. The predicted values are from the equation $X = a \log_{10}(OA_{initial}) + b(\text{Physical age}) + c$ where $X = \Delta f_{60}$, Δf_{44} , $\Delta O/\Delta C$, or \overline{D}_p . The values of a , b , and c are provided in Table S3. The Pearson and Spearman coefficients of determination (R_p^2 and R_s^2 , respectively) are provided in each panel, along with the normalized mean bias (NMB) and normalized mean error (NME). Note that Fig. 2 provides R values rather than R^2 to provide information upon the trend of the correlation. Included in the fit and figure are points from all four ΔCO regions within the plume (the 5-15%, 15-50%, 50-90%, and 90-100% of ΔCO), all colored by the mean $\Delta OA_{initial}$ of each ΔCO percentile range.